

# The interplay between ecological networks drives host-plasmid community dynamics

Ying-Jie Wang <sup>1,\*</sup>, Kaitlin Schaal <sup>2,†</sup>, Johannes Nauta <sup>3,†</sup>, Armun Liaghat <sup>4</sup>,  
Manlio De Domenico <sup>3</sup>, James Hall <sup>2</sup>, and Shai Pilosof <sup>1,\*</sup>

<sup>1</sup>Department of Life Sciences, Ben-Gurion University of the Negev, Beer-Sheva, Israel

<sup>2</sup>Department of Evolution, Ecology and Behaviour, Institute of Infection, Veterinary and Ecological Sciences, University of Liverpool, Liverpool L69 7ZB, UK

<sup>3</sup>Department of Physics and Astronomy Galileo Galilei, University of Padova, 35131 Padova, Italy

<sup>4</sup>Department of Ecology and Evolution, University of Chicago, Chicago, IL, USA

<sup>†</sup>Equal contribution

\*Corresponding authors: [yingjie@post.bgu.ac.il](mailto:yingjie@post.bgu.ac.il), [pilos@bgu.ac.il](mailto:pilos@bgu.ac.il)

## Abstract

Plasmids can accelerate host adaptation through horizontal gene transfer and are key members of microbial communities. Plasmid infection dynamics are potentially affected by the interplay between the structures of host-plasmid and plasmid-plasmid interactions. However, how the structures of these networks jointly affect plasmid transmission and community dynamics remains unstudied. We used an agent-based model to simulate the dynamics of a multihost-multipiasmid system in which we manipulated the structure of the ecological networks. The interplay between network structures affects host coexistence, population composition, and plasmid prevalence. For instance, plasmid incompatibility and a modular host-plasmid network promoted host coexistence. These effects were largely driven by the structure-induced dynamics of the co-infected individuals in microbial populations. A combination of modeling and a lab experiment further showed that the structure of the host-plasmid network determines plasmid fate. This study demonstrates how interactions between multiple ecological networks affect the dynamics and fate of infectious agents and their hosts. The structure of the ecological networks within microbial communities therefore has implications for the evolutionary potential of these communities.

## Introduction

Plasmids play a vital role in the eco-evolutionary dynamics of host communities. As extrachromosomal, semi-autonomous, mobile genetic elements (MGEs), plasmids can spread among host organisms, accelerating adaptation by transferring genes that confer advantageous traits such as antibiotic resistance [1–3]. Plasmids can also impose fitness costs on their hosts, which emerge from conflicts between chromosomal- and plasmid-encoded genes and the metabolic burdens of plasmid gene expression [4,5]. However, these cost-benefit interactions between plasmids and their hosts are deeply shaped by other microbiome interactions, such as plasmid co-infection and host competition, which together influence plasmid dynamics and the coexistence of their constituent hosts [6–12]. The impact of this interplay is often overlooked in studies of host-plasmid community dynamics.

Plasmids can interact with multiple hosts as they transfer across populations, creating patterns of host infection shaped by variation in within- and between-population conjugation rates, compatibility with host genetic backgrounds, and host anti-plasmid defense systems [13–15]. Plasmids can also compete with one another for hosts, using mechanisms such as (in)compatibility groups, toxin-antitoxin systems, and plasmid-encoded defense systems to exclude one another [16–22]. While some studies acknowledge the importance of multiple interaction types, they focus on simplified systems, such as multihost-uniplasmid [7] or unihost-biplasmid systems [8]. However, in nature, hosts and plasmids form complex structures of interactions [23]. The few studies which consider multihost-multiplasmid systems omit or understate plasmid co-infection, focusing on a single interaction type [24–26]. As a result, little is known about how the interplay of multiple interaction structures, specifically between host-plasmid interactions and plasmid co-infection, shapes community dynamics and stability. This gap in understanding hinders our ability to predict the assembly and evolutionary trajectories of these communities, particularly their potential in genetic innovation and adaptation. Nevertheless, addressing it is challenging because it requires connecting multiple and complex interaction types to dynamics.

The interplay of different interaction types can be studied using ecological networks, which encode interactions (links) between multiple species (nodes). Ecological networks are valuable tools for studying how network structure (i.e., the pattern in which interactions are distributed across species) affects community dynamics and species coexistence [27,28]. Considering multiple ecological networks allows us to study how distinct, interconnected networks affect community dynamics [12,29–31]. However, there is a paucity in studies that explicitly link dynamics to the interplay between networks, leading to a gap in our understanding of structure-dynamics in complex ecological communities.

In this work, we use host-plasmid interactions to address this gap. We investigated how host infection and plasmid compatibility networks jointly affect host and plasmid dynamics and coexistence. While other interaction types exist (e.g., host-host interactions such as competition [7,32] and horizontal gene transfer (HGT) [24,33]), we focus on infection (a host-plasmid interaction) and plasmid compatibility (a plasmid-plasmid-interaction, Fig. 1a) because these interactions are significantly understudied in a network context despite being fundamental to host-plasmid communities. We developed an agent-based model (ABM) (Fig. 1b) that incorporates the structure of both networks and simulates the dynamics of host and plasmid populations. Our model omits perturbations that provide plasmids with advantages (e.g., antibiotics against which plasmids can carry resistance genes), so that network structures can be compared within

a homogeneous abiotic environment. While the model is broadly applicable to systems of hosts and infectious agents, we focus on bacteria and plasmids throughout. We systematically vary the structures of the infection and plasmid compatibility networks to examine their individual and combined effects. Finally, we validate our model predictions using data from empirical laboratory experiments.

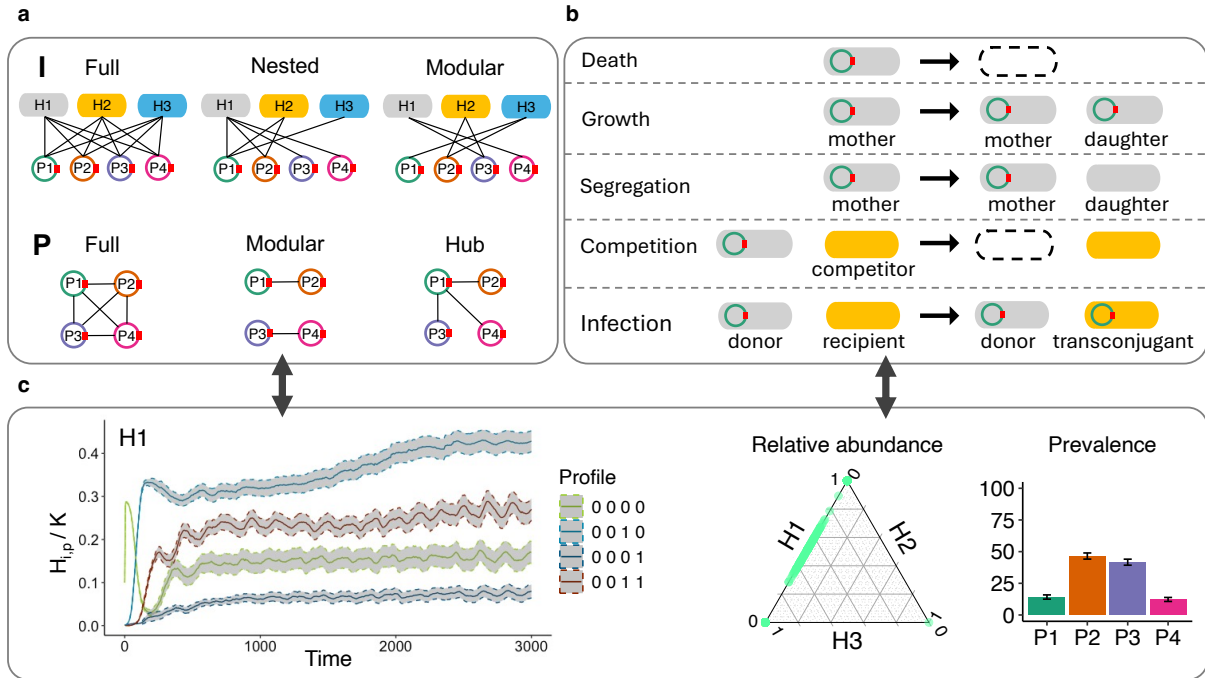


**Figure 1: Model overview and experimental design.** (a) The structures of the bacterial host-plasmid infection network **I** (which plasmid infect which hosts; top row) and plasmid-plasmid compatibility network **P** (which plasmids are compatible with each other and can therefore co-reside in a host individual; bottom row). The full structures serve as controls. We used a factorial experimental design of the nine structure combinations. (b) Illustration of the five main events in the ABM (see Methods for detailed model explanations). Dashed ovals indicate individual deaths. (c) An example of results of infection dynamics with modular **I** and full **P**, including subpopulation dynamics (left), final relative abundance of host populations of all replicates (middle), and the mean and SE of final plasmid prevalence across replicates at the end ( $t = 20000$  hours) of the simulation (right).

## Results

### Representing host-plasmid and plasmid-plasmid interactions using multiple ecological networks

To investigate how the interplay between ecological networks shapes dynamics, coexistence, and persistence within host-plasmid communities, we first defined typical structures for **I**, the host-plasmid infection network and **P**, the plasmid-plasmid compatibility network. To understand the relationship between network structure and dynamics in detail and from core principles, we intentionally used small networks (Fig. 1a). While this choice was primarily conceptual, focusing on tractability and interpretability, it also aligned with practical considerations, as simulating larger networks becomes computationally prohibitive (see Model limitations in Methods).

Previous studies of host-MGE infection networks have focused on phages, but similar principles can be used to represent host-plasmid interactions. Host-phage networks are bipartite

(contain two distinct sets of entities), and often exhibit modular and nested structures [12,34,35] (e.g., Fig. 1a, top row). Hence, for **I** we defined three possible structures: (1) ‘Full’, wherein all hosts can host all plasmids, serving as a reference (control). (2) ‘Nested’, wherein specialist plasmids interact with a subset of hosts with which more generalist plasmids interact [34–37]. Nestedness describes a hierarchical structure, and can arise if there is a trade-off between infecting multiple hosts and adapting to each host species [12,35,37] that leads to the evolution of a narrower host range. (3) ‘Modular’, wherein plasmid-host interactions form three distinct modules: two peripheral modules of hosts that infected by distinct subsets of plasmids, and a bridge module where hosts can host a subset of plasmids from each of the peripheral modules (Fig. 1a, top row). Host H2 and plasmids P2 and P3 in the bridge module are termed the bridge host and bridge plasmids. Modularity can arise from a phylogenetic HGT barrier, where HGT occurs more often between closely related species [38,39]. In our case, a modular structure arises when the bridge host is phylogenetically intermediate between the peripheral hosts, or when it lacks specific defenses to protect it from plasmid spillover from the peripheral hosts. Nestedness and modularity are signatures of host-MGE coevolution, where trade-offs between fitness and niche breadth result in specialization [12,35,37].

Plasmid-plasmid interactions can be represented as unipartite networks where nodes are plasmids and links indicate plasmid compatibility. Hence, two linked plasmids can co-reside in the same host (e.g., Fig. 1a, bottom row). While the structure of plasmid compatibility network **P** has received little attention, we defined three structures, based on theories in disease and community ecology: (1) ‘Full’, wherein all plasmids are compatible, serving as a reference (control). (2) ‘Modular’, wherein plasmids in the module are compatible with each other. Modularity can arise if the plasmids form (in)compatibility groups [18,20]. (3) ‘Hub’, wherein a sole hub plasmid is the only one compatible with others, while non-hub plasmids have few interactions and can co-reside with only a limited set of plasmids. Hub structures can arise from differences in plasmid traits that allow some plasmids to be widely compatible with each other or to complement each other functionally, similar to generalist parasites in disease ecology [40–43]. Notably, hub structures could lead to a disproportionately high prevalence of a few plasmids that may carry genes such as those conferring antimicrobial resistance.

## The model links host-plasmid dynamics with network structures

To understand how network structures affect population dynamics, we developed an agent-based model (ABM) that incorporates five demographic and stochastic events: growth, death, plasmid loss by segregation, competition between hosts, and plasmid transmission by conjugation (Fig. 1b). We employed a  $3 \times 3$  factorial experimental design of the **I** and **P** structures. In each experiment we tracked the quantity  $H_{i,p}$ , which is the abundance of a microbial host population  $i$  that can be infected with a combination of plasmids, forming subpopulations with a plasmid profile  $p$  (Fig. 1c). We included three hosts (H1-3) and four plasmids (P1-4). We used a binary notation system to describe the plasmid profile of each host subpopulation. For example, the total population abundance  $H_i = \sum_p H_{i,p}$  of a host  $i$  might be split into two subpopulations 0000 and 0011. The first subpopulation is plasmid-free and the second is infected with plasmids P3 and P4.

To focus on the effects of network structure, we assumed that all plasmids and host populations have identical traits (e.g., growth and death rates, conjugation rates). That is, host and plasmid types differ only in their niches (node position) in the interaction networks. We modeled host competition for a shared limiting resource by applying community-level density-dependent

growth (i.e. a community-wide carrying capacity) [44]. As such, we focus on cases where plasmids are costly, and do not consider the possible effects of perturbations. This choice allows us to isolate the structural effects on plasmid persistence and community dynamics from the effects of positive selection for plasmid-encoded traits. While plasmids often provide valuable traits enabling hosts to adapt to changes in the environment, understanding the maintenance of traits and the impact of plasmids in the absence of positive selection is important for assessing the resilience of communities to future perturbations, and plasmids have been shown to persist even in the absence of positive selection [10,17,45]. Therefore, the perturbation-free results we obtained enable a broad theoretical development regarding most infectious agents, which generally do not provide advantages to their hosts.

For each experiment, we calculated: (1) relative host abundance: the relative abundance of each host population out of the total community abundance; (2) plasmid prevalence: the fraction of host individuals across all populations which are infected with the plasmid; (3) host population composition: the proportions of subpopulations, each defined by a plasmid profile, within the host population; (4) host coexistence probability: the proportion of simulation replicates in which hosts coexisted at any given time point.

### Plasmid compatibility network structure promotes host coexistence

To understand the impact of the plasmid compatibility network  $\mathbf{P}$  on community dynamics, we compared community dynamics under various structures of  $\mathbf{P}$  while retaining a full infection network  $\mathbf{I}$ . Under full  $\mathbf{I}$  and full  $\mathbf{P}$ , only one host population survived (Fig. 2b(i), Fig. S1). The identity of the host varied stochastically across replicate simulations, and the overall probability of a specific host surviving was about 1/3, as expected. Throughout the simulation, the probability of host coexistence rapidly decreased to zero (Fig. 2b(i)). The host coexistence pattern was driven by neutrality and demographic stochasticity that eventually caused extinction, as well as by the high proportion of subpopulations infected by all four plasmids that induced multiplicative costs and sped up extinction (Fig. 2d(i); Fig. S2). These heavily infected subpopulations acted as main plasmid donors, continually re-infecting available hosts. At the final time point, all subpopulations (i.e., all possible plasmid profiles) of the surviving hosts were still present, and population composition was the same regardless of which specific host survived (Fig. 2d(i)). The four plasmids reached the same prevalence, infecting slightly more than half of the individuals of the sole surviving host (Fig. 2c(i)). This plasmid prevalence pattern was driven by all host individuals infected by one or multiple plasmids.

Introducing structure to plasmid compatibility drastically affected host coexistence patterns. When  $\mathbf{P}$  had a modular or hub structure, one host population still out-competed the other two by the end of the simulation, but the process took up to 3 times longer (Fig. 2b). The average prevalence of the plasmids was similar to each other under each  $\mathbf{P}$  structure, except for P1 infecting 100 % of its hosts as the hub plasmid (Fig. 2c(ii-iii)). We found a possible explanation for the prolonged host coexistence and the plasmid prevalence patterns by comparing the final population compositions to the full  $\mathbf{P}$  experiment (Fig. 2d). Infections with four plasmids were highly costly therefore accelerating extinction. In contrast to a full  $\mathbf{P}$ , under modular or hub  $\mathbf{P}$ , no host subpopulation could be infected with all four plasmids. Instead, the surviving host population in each replicate simulation was comprised solely of subpopulations infected by two plasmids (either the two plasmids that shared a module, or the hub plasmid and one other; Fig. 2d(ii-iii)). Structure in the plasmid compatibility network  $\mathbf{P}$  could therefore alter host dynamics through plasmid cost and patterns of conjugation. While all of the communities

ultimately collapsed to a single host population over the course of the simulations owing to the strict competition between hosts, **P** structures qualitatively altered plasmid fates and prolonged the period of host coexistence. In a natural community, these dynamic outcomes would provide greater opportunities for host and plasmid evolution.

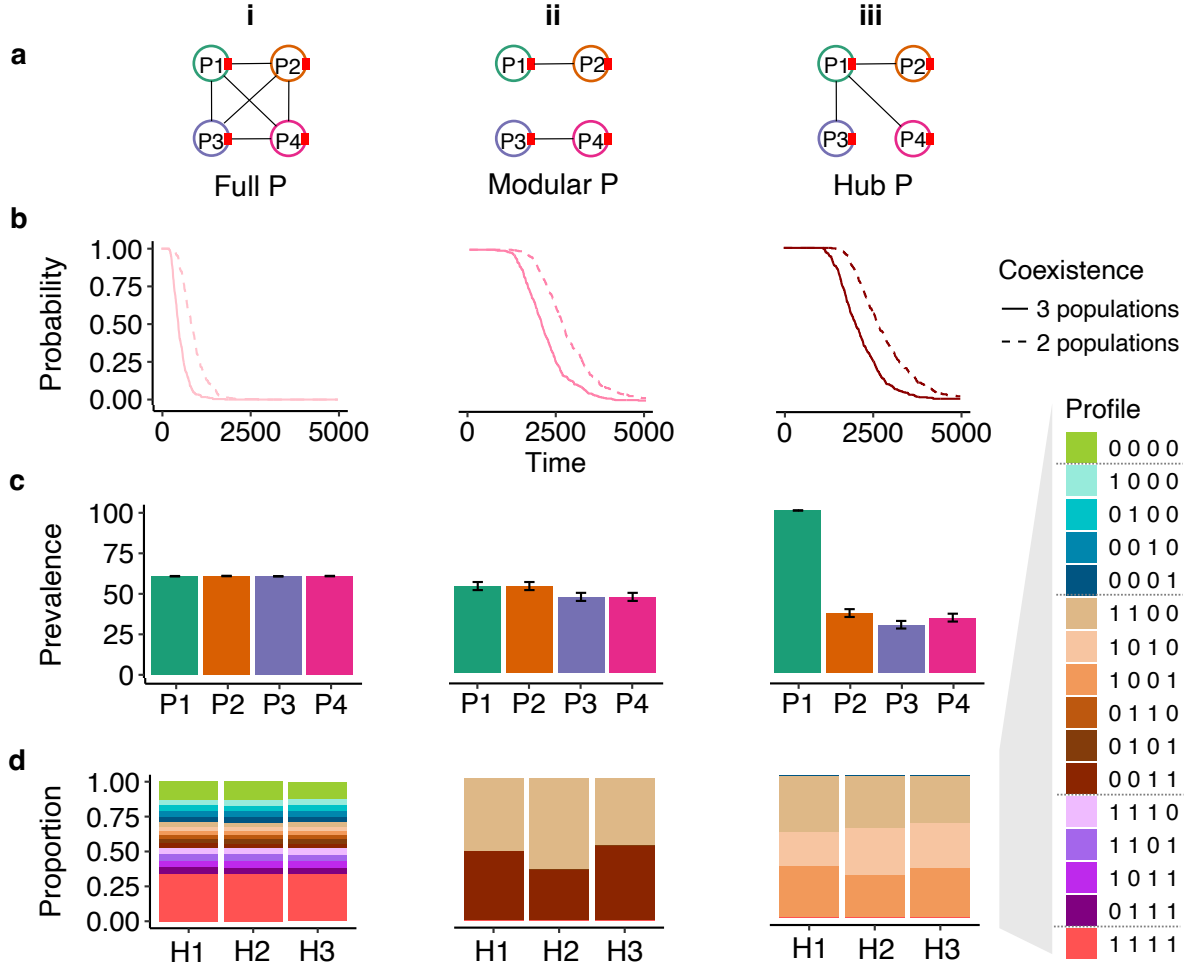


**Figure 2: The effect of structure in the plasmid compatibility network **P** under a full infection network **I**.** Columns i, ii, and iii represent different **P** structures. (a) Illustration of the different structures. (b) The dynamics of coexistence probability of host populations. (c) Mean and SE of final plasmid prevalence across all replicates. (d) Final host population composition, averaged across replicates in which that host population survived (only populations surviving in  $> 5$  replicates were considered). Profiles represent the host subpopulations (e.g., the profile 1000 represents a subpopulation hosting only P1).

### A modular infection network supports hosts and plasmid diversity

Next, we investigated the impact of infection network **I** on community dynamics. While under full **I**, each of the three host populations had an equal chance to out-compete the others in each simulation, under nested **I** (hierarchical infections) the plasmid-specialist host H3 consistently excluded the other two populations (Fig. 3b (i-ii)). As H3 could only be infected by the host-generalist P1, the other plasmids were lost from the community (Fig. 3c(ii)). This outcome resulted from the lower net fitness cost to H3 of being susceptible to only one plasmid (Fig. 3d(ii)); Fig. S3). A nested infection network should therefore be unlikely to be maintained without influence from external factors (see Discussion).

In contrast, a modular **I** was the only structure which enabled host coexistence. The peripheral hosts H1 and H3 were both present at the end of the simulation, while the bridge host H2 always went extinct (coexistence probability  $\approx 0.4$  vs. 0; Fig. 3b(iii); Fig. S4-Fig. S6). The rapid extinction of H2 was explained by it being quickly co-infected by P2 and P3, thus bearing a higher net fitness cost than populations H1 and H3 (otherwise it could survive, see column H2 in Fig. S7-Fig. S9). The bridge plasmids P2 and P3 had higher final prevalence than the peripheral plasmids P1 and P4 (Fig. 3c(iii)). P2 and P3 maintained higher prevalence throughout the simulation because earlier in the simulation when H2 was still present, it acted as a source and increased the rate at which H1 and H3 were infected by these bridge plasmids (Fig. S10). The longer-term success of P2 and P3 after their source H2 became extinct is an example of the long-term impact on communities caused by a transient, though unsuccessful population [46].

Overall, our results so far show that modular structures promote the maintenance of diversity. Specifically, we observed prolonged host coexistence with modular **P**, and stable host coexistence with modular **I**. Communities with such structures are therefore more likely to produce evolutionary innovation. However, our model also predicts that the loss of the bridge host H2 might impede plasmid evolution by restricting opportunities for recombination between the bridge plasmids.

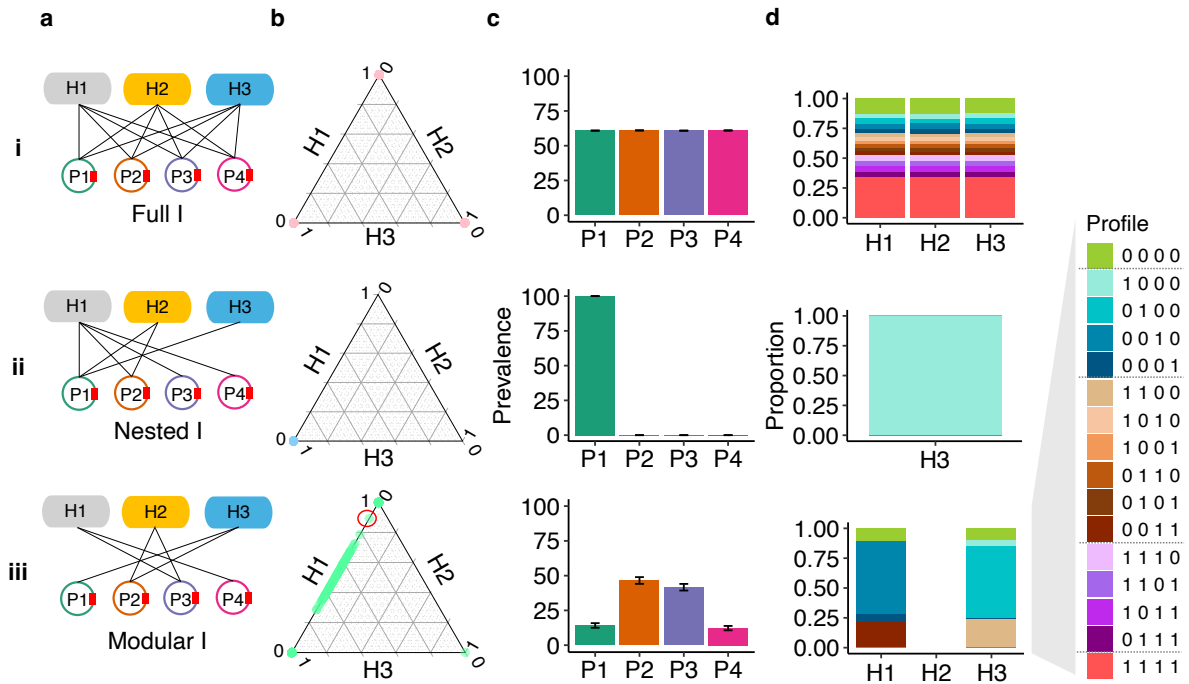


**Figure 3: The effect of structure in the infection network **I** under a full plasmid compatibility network **P**.** Rows i, ii, and iii represent different **I** structures. (a) Illustration of the structures of **I**. (b) Final relative abundance of host populations. Each dot represents a replicate. Dots on the vertices had no coexistence (i.e. only one population survived), while dots on the edges had coexistence of two populations. For example, the green dot marked with a red circle in b(iii) represents a community with relative abundances of 0.9 for H1, 0.1 for H2, and 0.0 for H3. (c) Mean and SE of final plasmid prevalence across all replicates. (d) Final host population composition, averaged across replicates in which that host population survived (only populations surviving in  $> 5$  replicates were considered). Profiles represent the host subpopulations (e.g., the profile 1000 represents a subpopulation hosting P1).

## Network structures can counteract the effects of one another

Up to this point, we explored structured **I** or **P** separately, while maintaining the other as a fully-connected control. In natural communities, structures likely exist in both of these networks simultaneously, so we next explored the interplay between the two. With a particular interest in the biological relevance of a hub structure, we demonstrate the results from a modular **I** and a hub **P** (see Fig. S1, S4, and S10 in [Supplementary Figures](#) for results from other combinations). In contrast with full **I**, where the hub plasmid P1 reached fixation (Fig. 2c(iii)), under modular **I** the hub plasmid P1 had a very low average final prevalence while P3 reached the highest average prevalence (Fig. 4c).

These patterns resulted from the interaction between the structures of **I** and **P**: although the hub plasmid P1 was compatible with the other three plasmids, the peripheral host H3 was its only possible host (Fig. 4a). H3 could therefore be co-infected by P1 and P2. Under a full **P**, the other peripheral host H1 could also be co-infected, but under a hub **P** this was no longer possible. This structure led to a higher net fitness of H1 compared to H3, driven by the co-infected subpopulation of H3. Consequently, H3 was less abundant than H1 on average across simulations, thereby limiting the abundance of P1 (Fig. 4b, d; Fig. S9). In addition, while under full **P** H2 always went extinct (Fig. 3b(iii)), under structured **P** it coexisted with host H3 in some simulations (Fig. 4b). This is because under structured **P** host H2 was not susceptible to the burden of co-infection (Fig. S9).

Overall, these results suggest that the infection network can counteract the effects of the plasmid compatibility network, especially when both are structured. Moreover, we expect that a hub plasmid compatibility structure—given as a boundary and initial condition that can be pruned by community dynamics—is unlikely to be maintained when paired with a modular infection structure, as a hub plasmid with a limited host range can rapidly reach low prevalence and therefore be lost stochastically from the community.

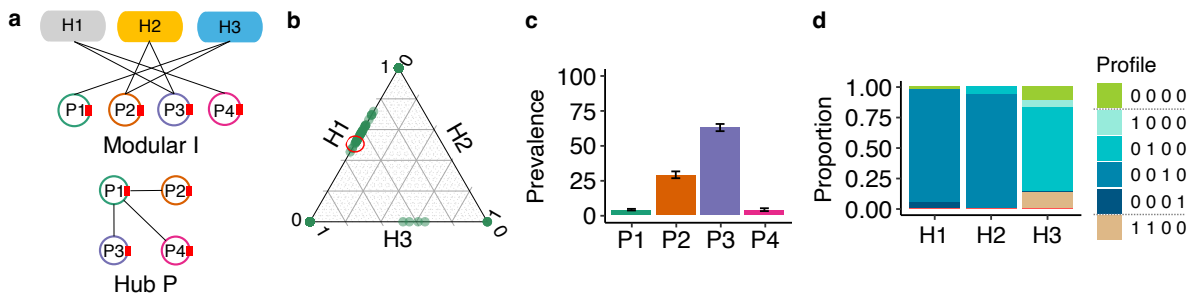


**Figure 4: The joint effect of structured networks: modular **I** and hub **P**.** (a) The modular network structure of infection **I** and the hub network structure of plasmid compatibility **P**. (b) Final relative abundance of host populations. Each dot represents a replicate. Dots on the vertices had no coexistence (i.e., only one population survives), while dots on the edges had the coexistence of two populations. For example, the green dot marked with a red circle represents a community with relative abundances of 0.5 for H1, 0.5 for H2, and 0.0 for H3. (c) Mean and SE of final plasmid prevalence across all replicates. (d) Final host population composition, averaged across replicates in which that host population survived (only populations surviving in  $> 5$  replicates were considered). Profiles represent the host subpopulations (e.g., the profile 1000 represents a subpopulation hosting P1).

## Infection network structure drives dynamics in an experimental system

To further investigate our theoretical predictions regarding the impact of a modular **I** structure on the community, we used an empirical system we developed [47]. The system comprised three

bacterial host populations and two plasmids distinguishable by their colony phenotypes. The size of our empirical system was limited by the fluorescent labels available to track the plasmids. The community consisted of *Pseudomonas fluorescens* SBW25 (bacterial host H1), *Pseudomonas putida* KT2440 (H2), and *Escherichia coli* MG1655 (H3). The plasmids were the *Pseudomonas*-specific, mercury-resistant plasmid pQBR57 (P1), and the antibiotic-resistant plasmid pKJK5 (P2) which, under the experimental conditions, was not able to conjugate into *P. fluorescens* SBW25. The system therefore can be described with a modular **I** and a full **P** (Fig. 5a).

As variation in quantitative trait values better aligns with the empirical system, we re-parameterized our model accordingly, using experimental measurements where possible (Table S1-Table S4, Supplementary Methods and Tables). Specifically, we used unequal population growth rates ( $H1 \leq H2 < H3$ ), infection rates ( $H1 = H2 < H3$ ), and plasmid costs ( $P1 < P2$ ), and a heterogeneous interspecific competition network ( $H1 < H2 < H3$ ). For computational tractability, we used lower values of community-wide carrying capacity ( $K_{ABM} = 10^5$  vs  $K_{empirical} = 10^9$ ) and initial abundances ( $B_{0ABM} = 3.3 \times 10^3$  vs  $B_{0empirical} = 3.3 \times 10^5$  for each population). These differences did not affect the qualitative dynamics, and we compared empirical and model values in relative terms.

Following our theoretical results, we expected that under a modular **I** and a full **P** that the bridge host H2 would be outcompeted by the peripheral hosts and go extinct, and that the resulting community would be primarily composed of infected subpopulations (Fig. 3d(iii)). In contrast to this prediction, H2 maintained a higher relative abundance than the peripheral host H1 (Fig. 5b). The most abundant plasmid in the system was P2, following the high abundance of its host (Fig. 5c). The differences between the theory and the experiment may be explained by the heterogeneous growth rates, the interspecific competition network, and an increase in the growth rate of the bridge host. Indeed, when these factors were considered in the model (Table S1), the simulations qualitatively reflected the experimental results (Fig. 5b-e, Fig. S11).

The key insight of our model is that structure in the **I** and **P** networks affects community dynamics. Having recapitulated the empirical results, we used the re-parameterized model to test how the outcome would change given an unstructured infection network (full **I**; Fig. 5f). While the host population dynamics remained unchanged (Fig. 5g), the subpopulation dynamics were strikingly and qualitatively different. Specifically, the less costly plasmid P1 reached a higher community-wide prevalence instead of P2 (Fig. 5h). This provided further support that network structure is a key contributor to plasmid dynamics in natural systems.

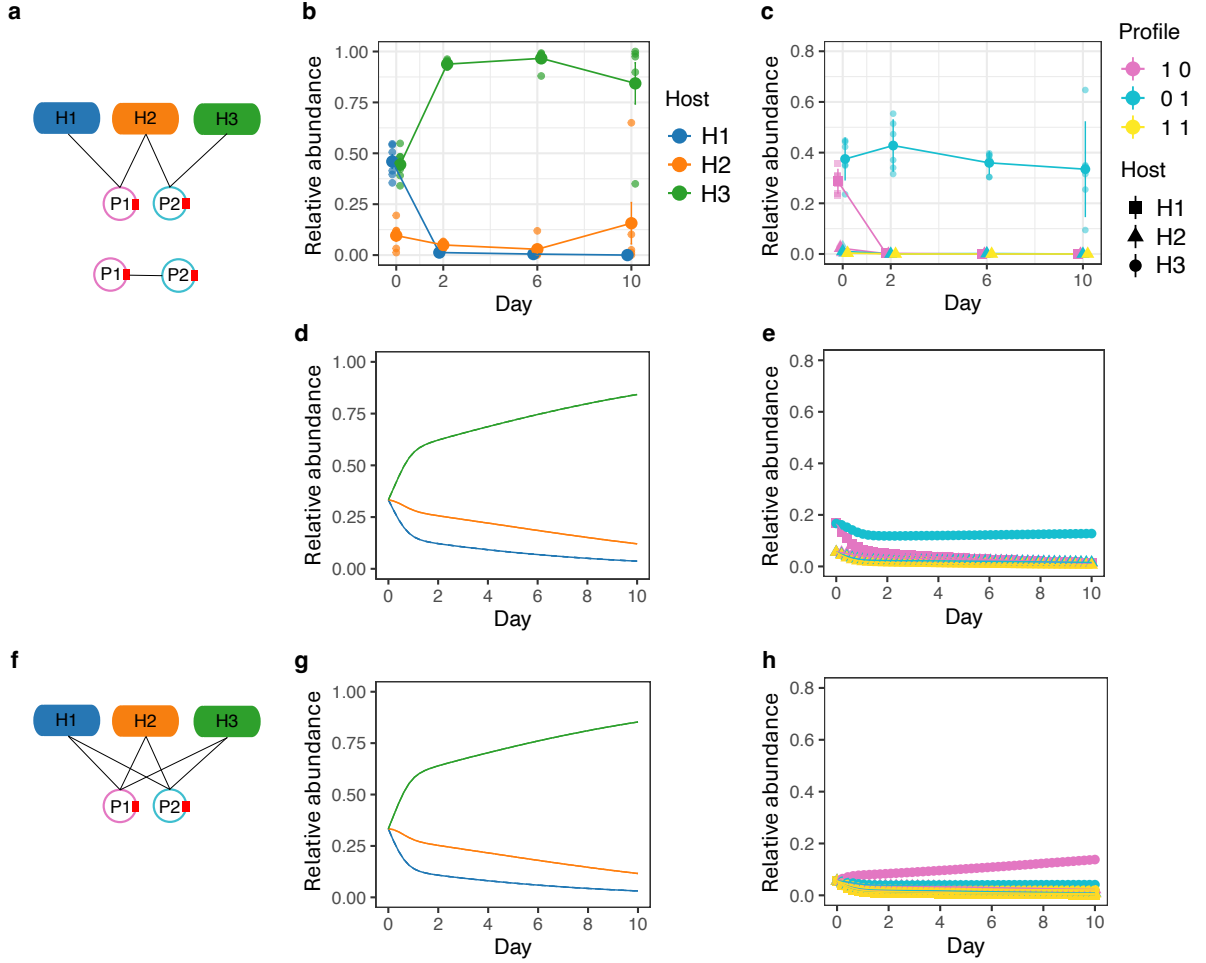


**Figure 5: Empirical network structures and simulated population dynamics.** (a) Empirical infection network  $\mathbf{I}$  (top) and plasmid compatibility network  $\mathbf{P}$  (bottom) from the empirical system. (b) Host population dynamics in the empirical system. (c) Infected subpopulation (plasmid) dynamics in the empirical system. (d) Simulated host population dynamics using the empirical networks. (e) Simulated infected subpopulation dynamics using the empirical networks. The empirical and modeling systems show similar patterns for host (panel b vs panel d) and plasmid (panel c vs panel e) dynamics. (f) Full infection network  $\mathbf{I}$  used in simulation. (g) Simulated host population dynamics under the full infection network. (h) Simulated infected subpopulation dynamics under the full infection network. Using a full infection network (panel f) resulted in similar host population dynamics (panel g) but qualitatively different plasmid dynamics (panel h). All abundances are relative to community size. Error bars represent SE. The empirical observations had a sample size of 6, while the ABM simulations had a sample size of 300.

## Discussion

Network structures underlying microbial interactions fundamentally shape community dynamics, yet the interplay of distinct networks remains poorly understood. Our work highlights how the combined effects of host-plasmid infection and plasmid-plasmid compatibility networks determine microbial coexistence and plasmid prevalence, potentially shaping long-term evolutionary trajectories. We show that a structured infection network exerts a stronger influence on host and plasmid persistence than a structured compatibility network. However, compatibility patterns still play a crucial role in shaping plasmid diversity and co-infection dynamics, which in turn influence plasmid recombination and evolutionary innovation [3].

An important finding is that the infection network retains its modular structure more con-

sistently when the plasmid compatibility network is also structured, underscoring a rarely considered mechanism: the interplay between structured networks itself enhances stability. This observation reinforces the necessity of considering interactions between multiple networks when investigating the ecology of infectious agents. Empirical studies support this idea, as structured infection networks often co-occur with restricted plasmid transfer pathways, limiting the spread of deleterious plasmids [26]. Moreover, our model-derived insight that plasmid compatibility shapes host persistence finds support in studies where host-plasmid dynamics are influenced by both direct host interactions and compatibility constraints [22]. Future empirical work should aim to test whether structured plasmid compatibility networks similarly increase the stability of community composition and function in natural microbial communities.

Our results indicate that a structured plasmid compatibility network alters host population composition. Therefore, the structure of the compatibility network can determine plasmid recombination potential [18]. Such structure-dynamics feedback can have implications for multidrug resistance, which emerges primarily through horizontal gene transfer between compatible plasmids in the same host [48,49]. Empirical evidence suggests that MGEs can actively rewire compatibility networks by interfering with competing elements [22], reinforcing our finding that compatibility constraints limit the range of hosts a plasmid can inhabit, thereby shaping host-plasmid interactions. Our results also indicate that plasmids are more likely to persist than hosts under changing network structures if they can survive in a single surviving host population. Thus, plasmids have substantial potential for evolution and host range expansion even under reduced host diversity, mirroring real-world observations of broad-host-range plasmids [5].

Unlike compatibility networks, structured infection networks led to strong heterogeneity in plasmid prevalence across plasmids and in co-infection across hosts. This was also supported by the version of the model parameterized according to the experimental data, where the infection network structure qualitatively changes plasmid fates. In contrast to plasmid compatibility networks, infection networks in our model were inherently unstable, frequently leading to host extinction. This contrasts with natural systems, where modular and nested structures are commonly observed [34,36,50], suggesting stabilizing factors. Population-level trait heterogeneity and positive epistasis in plasmid fitness costs [8,17] may mitigate destabilization, allowing structured networks to persist in nature. The asymmetry between host and plasmid dynamics arises because altered plasmid compatibility can expose hosts to a high infection burden, leading to their extinction, while changes in infection patterns are less likely to cause plasmid extinction as long as a viable host remains.

Our study focused on a small and fixed system to isolate effects related to network structure. Yet, in larger systems, functional redundancy and increased complexity of interactions could dampen the effects of network interplay [51–53]. We further assumed uniform host traits as well instead of introducing host diversity. While previous studies suggest that host heterogeneity does not critically alter horizontal gene transfer patterns [24], incorporating host heterogeneity could alter our predictions. Nevertheless, we note that parameterizing our model according to empirical data did not qualitatively change the key result that structure alters plasmid dynamics. Finally, we did not consider perturbations such as antibiotic stress, which—as shown in an empirical experiment [47]—can shift host-MGE interactions from antagonistic to mutualistic. While this allowed us to generate a theory that is generally relevant for infectious agents, future research could integrate eco-evolutionary feedback and perturbations to capture these dynamical aspects of host-plasmid communities.

An open question is how network structure evolves and persists. While the infection and com-

patibility networks we modeled resemble those observed in microbial ecosystems [12,34,35,40–43], we effectively treated them as boundary conditions within which links can change but nodes themselves cannot evolve. In reality, network structures emerge via eco-evolutionary processes [12,23,36] and host adaptation, immunity, and plasmid evolution likely shape infection network structure [23,35]. Plasmid compatibility networks, although much less studied, likely evolve through recombination [3] and mutations [54]. Adaptive defense mechanisms that mediate plasmid competition [21,22] may also influence compatibility constraints. Moreover, there may be interacting evolutionary trajectories of the interacting networks, leading to multi-level selection. Future models could incorporate such evolutionary feedback, shifting from fixed boundary conditions to dynamic, emergent structures.

In conclusion, our study provides a novel perspective on microbial ecology by explicitly demonstrating that the interplay between host-plasmid infection and plasmid-plasmid compatibility networks profoundly shapes community dynamics and evolutionary potential. Crucially, we find that the interconnectedness of these ecological networks itself stabilizes host-plasmid communities, underscoring the need to move beyond studying interaction types in isolation. Beyond microbial ecology, these theoretical and modeling developments offer insights into community dynamics of infectious agents and their hosts.

## Methods

### Host-plasmid agent-based model

#### Entities

The entities (agents) of the ABM were host subpopulations. Each subpopulation of host  $i$  contained a plasmid profile  $p$ . Each plasmid profile is a vector of elements 0 and 1, representing the presence (1) or absence (0) of each plasmid in the subpopulation. Therefore, a community with  $n_b$  hosts and  $n_p$  plasmids had at most  $n_b \times 2^{n_p}$  subpopulations. We defined  $H_{i,p}$  as the abundance of a subpopulation, and  $H_i$  as the abundance of host  $i$  ( $H_i = \sum_{p=\mathbf{0}}^{2^{n_p}-1} H_{i,p}$ ). For simplicity, we assumed each plasmid had a single copy in each host individual. We present an example for this notation in Table 1. Based on the plasmid profiles, we generated a list of donors (the plasmid-infected subpopulations that can transmit plasmids to others), and for each donor a list of recipients (the subpopulations that can receive plasmids from the donor) during ABM initialization. The lists of donors and recipients were used to sample subpopulations that undergo HGT and were updated during the simulations when new subpopulations emerged.

**Table 1: Example of agent notation.** In this example there are hosts (H1 and H2) and two plasmids (P1 and P2).

Host ( $i$ )	Plasmid profile ( $p$ )	Abundance ( $H_{i,p}$ )
1	[0,0]	10
1	[1,0]	5
1	[0,1]	0
1	[1,1]	0
2	[0,0]	10
2	[1,0]	5
2	[0,1]	0
2	[1,1]	0

## Spatial and temporal scales

We did not consider a spatial structure. We used hour as the time unit, as most per-capita rates are quantified with this unit in microbial studies. We used a 20000 hours time span for the simulations of the theoretical part to ensure stable coexistence, and a 240 hours (10 days) time span for simulations supporting the lab experiment, which is ample for most host populations/communities to reach carrying capacity in a lab environment [10].

## Events

Five major events contributed to the dynamics of the entities: death, growth, segregation, competition, and infection (Fig. 1b). In each death and competition event, the chosen agent decreased its abundance by one. In each growth event, the chosen agent increased its abundance by one. In each segregation event (i.e., growth with segregation error), we assumed plasmid segregation fails, so the plasmid-free agent  $H_{i,0}$  increased its abundance by one. With each infection event, the chosen donor agent  $H_{i,p}$  infected a recipient agent  $H_{k,q}$ , turning it into a transconjugant agent  $H_{k,r}$ . As a result, the donor’s abundance remained the same, the recipient’s abundance decreased by one, and the transconjugant’s abundance increased by one.

## Parameters

**Interaction networks** We used an infection network and a plasmid compatibility network. The infection network  $\mathbf{I}$  was a binary incidence matrix that determined if the plasmid  $\beta$  (column) can infect the host  $i$  (row). The plasmid compatibility network  $P$  was a symmetric binary matrix that determined if two plasmids  $\alpha$  and  $\beta$  can coexist within the agent individuals, with the assumption that plasmids were self-incompatible ( $P_{\alpha\beta} = 0 \forall \alpha = \beta$ ). We also assumed that the hosts had equal strength of interspecific competition, and that HGT occurred both between and within hosts.

**Host and plasmid traits** For the host, we used per capita growth rate  $\eta_i$ , per capita death rate  $\mu_i$ , and probability of segregation error  $e_i$ . For the plasmids, we used plasmid cost on host growth  $c_\alpha$ . We applied a community-wide carrying capacity  $K$ , limiting the sum of population abundances. A complete list of parameters and their values is provided in Table 2

**Table 2:** Parameter values used in the simulations of the theoretical part. Parameter values were based on/taken from [55].

Host traits	H1	H2	H3	
growth rate $\eta_i$	1	1	1	
death rate $\mu_i$	0.12	0.12	0.12	
infection rate $\gamma_i$	$10^{-5}$	$10^{-5}$	$10^{-5}$	
segregation rate $\gamma_i$	$10^{-8}$	$10^{-8}$	$10^{-8}$	
community-wide carrying capacity $K$	20000	20000	20000	
intraspecific competition coefficient $a_{ii}$	1	1	1	
interspecific competition coefficient $a_{ij}$	0.01	0.01	0.01	
Plasmid traits	P1	P2	P3	P4
plasmid cost $c_\alpha$	0.3	0.3	0.3	0.3

**Infection propensity** When the infection event is chosen, we considered the propensities with which transconjugants were generated given combinations of donors and recipients. Specifically,

we used a three-dimensional infection propensity tensor  $\Gamma$ , with each dimension of size  $n_b^{n_p}$  corresponding to all potential entities (subpopulations)  $H_{i,p}$  along the transconjugant, donor, and recipient axes. We assumed that the more plasmids transmitted in an infection, the lower the propensity. Thus, the elements (propensities) of  $\Gamma$  that met the infection conditions (Table 3) were estimated following the power law:

$$\Gamma_{k,r;i,p;k,q} = \frac{1}{2^{\nu-1}}, \quad (1)$$

Here,  $\Gamma_{k,r;i,p;k,q}$  represented the propensity of the recipient  $H_{k,q}$ , after receiving plasmid(s) from donor  $H_{i,p}$ , to become transconjugant  $B_{k,r}$ . The parameter  $\nu$  represented the number of plasmid strains being transferred from the donor to the recipient. Other elements of  $\Gamma$  were treated as 0. We provide an example propensity tensor for a system with one host and two plasmids in Fig. 6.

**Table 3:** Conditions for infection to occur.

Condition	Content
1	Donor is plasmid-infected ( $p \neq \mathbf{0}$ )
2	Donor has plasmid(s) that the recipient does not
3	Transferable plasmid(s) can infect the recipient ( $\mathbf{I}_{\beta i} = 1$ )
4	Plasmids in the transconjugant can coexist ( $\mathbf{P}_{\alpha\beta} = 1$ )

		Recipient = $H_{1,[0,0]}$			
Transconjugant	$H_{1,[0,0]}$	0	0	0	0
	$H_{1,[1,0]}$	0	1	0	1
	$H_{1,[0,1]}$	0	0	1	1
	$H_{1,[1,1]}$	0	0	0	1/2
		$H_{1,[0,0]}$	$H_{1,[1,0]}$	$H_{1,[0,1]}$	$H_{1,[1,1]}$
		Donor			

**Figure 6: An example for a propensity tensor.** This example focuses on the dimension of the recipient  $H_{k=1,q=[0,0]}$ . Element  $\Gamma_{1,[1,1];1,[1,1];1,[0,0]} = 1/2$  because there are two plasmids being transferred from the donor  $H_{i=1,p=[1,1]}$  to the recipient  $H_{k=1,q=[0,0]}$ , creating the transconjugant  $H_{k=1,r=[1,1]}$ . Each column of the propensity tensor (i.e., with a given combination of donor and recipient) with at least one element  $> 0$  was then normalized to 1, ensuring the propensities of each column summed up to 1.

## Rates

The dynamics of the subpopulations were based on a Lotka-Volterra model with infection-recovery elements. In this model, each subpopulation had its per capita rate of events based on strain and plasmid profile, and its total rates of events based on its per capita rates  $\times$  abundance, which summed up to the total rate of events  $R$ . Below we define the equations of subpopulation per capita rates (variables used in the equations are described in Table S5, Supplementary Methods and Tables). We defined the subpopulation per capita death rate as  $\mu_{i,p} = \mu_i$  (host-specific) and the per capita growth rate as

$$\eta_{i,p} = \eta_i \prod_{\alpha|p_\alpha \neq 0} (1 - c_\alpha), \quad (2)$$

where the realized growth rate was the host-specific per capita growth rate,  $\eta_i$ , times the product of the complements of the costs across plasmids hosted by the subpopulation. Therefore, we assumed that the plasmid costs are not additive but multiplicative for the host. We defined the subpopulation per capita segregation rate as

$$\omega_{i,p} = e_i \eta_{i,p}. \quad (3)$$

We defined the competition matrix  $\mathbf{A}$ , in which each cell  $a_{ij}$  is the effect of host  $j$  on the per capita growth rate of host  $i$ . As with other parameters, we used a uniform  $a_{ij} = 0.01$  to ensure that the community effects we get are not due to some random competitive advantage of one host over another, but rather due to the structure of the networks. We applied a community-wide carrying capacity  $K$ , and defined the subpopulation per capita competition rate as

$$\xi_{i,p} = \eta_{i,p} \left( \sum_j H_{ij} \frac{H_j}{K} \right). \quad (4)$$

Here,  $H_{ij} = a_{ij} + 1$  for  $i \neq j$ , and  $a_{ij}$  equals to 1 when  $i = j$ .

We defined the subpopulation per capita infection rate  $\phi_{i,p}$  as

$$\phi_{i,p} = \gamma_{i,p} \sum_{\mathbf{G}} H_{i,p} \in \mathbf{G}, \quad (5)$$

where  $\gamma_{i,p}$  is the per capita encounter rate between a donor (i.e., plasmid-hosting) and its recipients, and was either host-specific for subpopulations hosting plasmid(s), or zero for the plasmid-free subpopulations.  $\mathbf{G}$  was the set of recipient subpopulations that could receive plasmid(s) from the donor subpopulation. While the mechanisms by which the donors and recipients of plasmids meet could be complex [56], we assumed these mechanisms to be donor-dependent and plasmid-profile-independent.

## Simulations

We applied the Gillespie algorithm, which includes the following steps:

1. Initialize the system with variable inputs (including parameter values and initial subpopulation abundances) (Table S6, Supplementary Methods and Tables), and set time  $t$  to zero.
2. Calculate the total rate of the system  $R = R_D + R_G + R_S + R_C + R_I$ , which is composed of the total rates of death:

$$R_D = \sum_{i,p} \mu_{i,p} H_{i,p}, \quad (6)$$

growth:

$$R_G = \sum_{i,p} \eta_{i,p} H_{i,p}, \quad (7)$$

segregation:

$$R_S = \sum_{i,p} \omega_{i,p} H_{i,p}, \quad (8)$$

competition:

$$R_C = \sum_{i,p} \xi_{i,p} H_{i,p}, \quad (9)$$

and infection:

$$R_I = \sum_{i,p} \phi_{i,p} H_{i,p} \quad (10)$$

3. Sample the length of a time step  $\Delta t = \frac{X}{R}$ , where  $X$  was drawn from an exponential distribution with a mean of 1.
4. Randomly sample an event, with weights proportional to the event's weight out of the total rate ( $R_D/R, R_G/R, R_S/R, R_C/R, R_I/R$ )
5. Sample the agent(s). If the chosen event is not infection, randomly sample an agent  $H_{i,p}$ , with weights according to the subpopulations' event rates. If the chosen event is infection, first sample a donor agent  $H_{i,p}$  from the plasmid-infected subpopulations, with weights according to their infection rates. Then, sample a recipient agent  $H_{k,q}$  from the recipient subpopulations that are vulnerable to the donor, with weights according to their abundances. Finally, sample a transconjugant agent  $H_{k,r}$ , with weights according to the propensity tensor  $\mathbf{\Gamma}$ .
6. Execute the chosen event for the chosen agent(s), and update the simulation time ( $t' = t + \Delta t$ ).
7. Move to step 3 until the simulation time meets the final time. Meanwhile, record the subpopulation abundances when  $t$  is equal to or passes desired length of time set for recording the system's set (5 hours in our case).
8. When the simulation reaches the defined time limit  $t = 20000$  or  $t$  at which the system collapses (all host populations have zero abundance), write the data frame into the output file in SQLite format. The output file was used for further analyses.

## Model limitations

Although our model can simulate multihostmultiplasmid systems, it faces computational constraints as system complexity increases. As the number of host ( $n_b$ ) and plasmid populations ( $n_p$ ) increases, so does the time required to generate the infection propensity tensor (of size  $n_b \times 2^{n_p}$  in each of the three dimensions), and to initialize the system (e.g., generate lists of donors and corresponding recipients) unless the interaction networks are extremely sparse. Because the Gillespie algorithm is used, increasing system complexity and community-wide carrying capacity inevitably raises the total event rate  $R$ . This, in turn, reduces the sampled time step in each iteration, making it more time-consuming for the simulation to reach the final time (Fig. S13, [Supplementary Methods and Tables](#)).

## Experimental design of the theoretical part

We used a  $3 \times 3$  factorial design of the combinations of  $\mathbf{I}$  and  $\mathbf{P}$ , which resulted in 9 experiments (Table 4). Due to the stochastic nature of the ABM, we ran 300 replicates for each experiment, each with a different seed for random sampling. To test how plasmids spread, we initiated populations with a low abundance of monoplasmidic subpopulations (10) compared to plasmid-free subpopulations (2000). We included all potential monoplasmidic subpopulations, so that each plasmid already existed in focal hosts before it was acquired from other hosts.

**Table 4:** Experimental design of the theoretical part.

Expt.(code)	I	P
1 (FF)	full	full
2 (FM)	full	modular
3 (FH)	full	hub
4 (NF)	nested	full
5 (NM)	nested	modular
6 (NH)	nested	hub
7 (MF)	modular	full
8 (MM)	modular	modular
9 (MH)	modular	hub

## Lab experiment

We used data from the study by Schaal et al. [47], which contains a detailed description of the experiment. Briefly, a community of three host bacteria (*Pseudomonas fluorescens* SBW25, *Pseudomonas putida* KT2440, and *Escherichia coli* MG1655) and two plasmids (the mercury-resistant pQBR57, and the antibiotic-resistant plasmid pKJK5) was cultured over five 48-hour transfers (10 days) in shaken liquid medium. One host could be (co)-infected by both plasmids, while the other two hosts could only be infected by one plasmid each (Fig. 5a). In this work, we used the data only from the communities that did not experience environmental stress. We used bacterial derivatives and fluorescent proteins to track different host populations and plasmids, and applied a link-balanced initial community composition, where all populations started with equal abundance, comprising of 50% plasmid-free subpopulation and 50% plasmid-carrying subpopulations. We quantified population and subpopulation abundance on days 2, 6, and 10, and summarized population and subpopulation dynamics.

## Code availability

The code for ABM simulation, input generation, output analyses, and empirical data analysis is available in the dedicated Github repository associated with this paper at: [https://github.com/HFSP-EcoNets/ABM\\_code](https://github.com/HFSP-EcoNets/ABM_code).

## Data availability

Simulated data is available in the dedicated Github repository associated with this paper at: [https://github.com/HFSP-EcoNets/ABM\\_code](https://github.com/HFSP-EcoNets/ABM_code). Empirical data is available in the dedicated Github repository associated with the collaborative study by Schaal et al. [47].

## Acknowledgments

We thank G. Galai for technical support in programming. Prof. David Alonso and Prof. Mercedes Pascual provided insightful comments.

## Funding

The study was funded by the Human Frontiers Science Program (grant RGY0064/2022) to SP, JPH, MDD. Kreitman school of Advanced Graduate Studies, Ben-Gurion University of Negev, supported the salary of YJ.

## Author contributions

Y.-J.W., K.S., J.N., M.D.D., J.P.H., and S.P. conceptualized the research. Y.-J.W., K.S., J.N., and S.P. designed the methodology. Y.-J.W., J.N., and A.L. developed the software. Y.-J.W. performed validation, formal analysis, data curation, and visualization. Y.-J.W., K.S., J.N., J.P.H., and S.P. wrote the original draft. Y.-J.W., K.S., J.N., A.L., M.D.D., J.P.H., and S.P. reviewed and edited the manuscript. M.D.D., J.P.H., and S.P. supervised the project. S.P. managed project administration. M.D.D., J.P.H., and S.P. acquired funding.

## Competing interests

The authors declare no competing interests.

## References

1. Smalla Kornelia, Jechalke Sven & Top Eva M. Plasmid Detection, Characterization, and Ecology. *Microbiology Spectrum* **3**, 10.1128/microbiolspec.plas-0038-2014. doi:[10.1128/microbiolspec.plas-0038-2014](https://doi.org/10.1128/microbiolspec.plas-0038-2014) (2015).
2. San Millan, A. Evolution of Plasmid-mediated antibiotic resistance in the clinical context. *Trends Microbiol.* **26**, 978–985. doi:[10.1016/j.tim.2018.06.007](https://doi.org/10.1016/j.tim.2018.06.007) (2018).
3. Rodriguez-Beltrn, J., DelaFuente, J., Len-Sampedro, R., MacLean, R. C. & San Milln., Beyond horizontal gene transfer: the role of plasmids in bacterial evolution. *Nat. Rev. Microbiol.* **6**, 347–359. doi:[10.1038/s41579-020-00497-1](https://doi.org/10.1038/s41579-020-00497-1) (2021).
4. San Millan, A. & MacLean, R. C. Fitness Costs of Plasmids: a Limit to Plasmid Transmission. *Microbiology Spectrum* **5**. doi:[10.1128/microbiolspec.mtbp-0016-2017](https://doi.org/10.1128/microbiolspec.mtbp-0016-2017) (2017).
5. Hall, J. P. J. *et al.* Plasmid fitness costs are caused by specific genetic conflicts enabling resolution by compensatory mutation. *PLoS Biol.* **19**, e3001225. doi:[10.1371/journal.pbio.3001225](https://doi.org/10.1371/journal.pbio.3001225) (2021).
6. Ghoul, M. & Mitri, S. The ecology and evolution of microbial competition. *Trends Microbiol.* **24**, 833–845. doi:[10.1016/j.tim.2016.06.011](https://doi.org/10.1016/j.tim.2016.06.011) (2016).
7. Coyte, K. Z. *et al.* Horizontal gene transfer and ecological interactions jointly control microbiome stability. *PLoS Biol.* **20**, e3001847. doi:[10.1371/journal.pbio.3001847](https://doi.org/10.1371/journal.pbio.3001847) (2022).
8. Iglér, C., Huisman, J. S., Siedentop, B., Bonhoeffer, S. & Lehtinen, S. Plasmid co-infection: linking biological mechanisms to ecological and evolutionary dynamics. *Philos. Trans. R. Soc. Lond. B Biol. Sci.* **377**, 20200478. doi:[10.1098/rstb.2020.0478](https://doi.org/10.1098/rstb.2020.0478) (2022).
9. Dewan, I. & Uecker, H. A mathematician’s guide to plasmids: an introduction to plasmid biology for modellers. *Microbiology* **169**. doi:[10.1099/mic.0.001362](https://doi.org/10.1099/mic.0.001362) (2023).

10. Hall, J. P. J., Jamie Wood, A, Harrison, E. & Brockhurst, M. A. Source–sink plasmid transfer dynamics maintain gene mobility in soil bacterial communities. *Proc. Natl. Acad. Sci. U. S. A.* **113**, 8260–8265. doi:[10.1073/pnas.1600974113](https://doi.org/10.1073/pnas.1600974113) (2016).
11. Kottara, A., Carrilero, L., Harrison, E., Hall, J. P. J. & Brockhurst, M. A. The dilution effect limits plasmid horizontal transmission in multispecies bacterial communities. *Microbiology* **167**. doi:[10.1099/mic.0.001086](https://doi.org/10.1099/mic.0.001086) (2021).
12. Pilosof, S. *et al.* The network structure and eco-evolutionary dynamics of CRISPR-induced immune diversification. *Nat Ecol Evol* **4**, 16501660. doi:[10.1038/s41559-020-01312-z](https://doi.org/10.1038/s41559-020-01312-z) (2020).
13. Alderliesten, J. B. *et al.* Effect of donor-recipient relatedness on the plasmid conjugation frequency: a meta-analysis. *BMC Microbiol.* **20**, 135. doi:[10.1186/s12866-020-01825-4](https://doi.org/10.1186/s12866-020-01825-4) (2020).
14. Deep, A. *et al.* The SMC-family Wadjet complex protects bacteria from plasmid transformation by recognition and cleavage of closed-circular DNA. *Mol. Cell* **82**, 4145–4159.e7. doi:[10.1016/j.molcel.2022.09.008](https://doi.org/10.1016/j.molcel.2022.09.008) (2022).
15. Jasklska, M., Adams, D. W. & Blokesch, M. Two defence systems eliminate plasmids from seventh pandemic *Vibrio cholerae*. *Nature* **604**, 323–329. doi:[10.1038/s41586-022-04546-y](https://doi.org/10.1038/s41586-022-04546-y) (2022).
16. Novick, R. P. Plasmid incompatibility. *Microbiol. Rev.* **51**, 381–395. doi:[10.1128/mr.51.4.381-395.1987](https://doi.org/10.1128/mr.51.4.381-395.1987) (1987).
17. San Millan, A., Heilbron, K. & MacLean, R. C. Positive epistasis between co-infecting plasmids promotes plasmid survival in bacterial populations. *ISME J.* **8**, 601–612. doi:[10.1038/ismej.2013.182](https://doi.org/10.1038/ismej.2013.182) (2014).
18. Dionisio, F., Zilho, R. & Gama, J. A. Interactions between plasmids and other mobile genetic elements affect their transmission and persistence. *Plasmid* **102**, 29–36. doi:[10.1016/j.plasmid.2019.01.003](https://doi.org/10.1016/j.plasmid.2019.01.003) (2019).
19. Cooper, T. F. & Heinemann, J. A. Postsegregational killing does not increase plasmid stability but acts to mediate the exclusion of competing plasmids. *Proc. Natl. Acad. Sci. U. S. A.* **97**, 12643–12648. doi:[10.1073/pnas.220077897](https://doi.org/10.1073/pnas.220077897) (2000).
20. Helinski, D. R. A Brief History of Plasmids. *EcoSal Plus* **10**, eESP00282021. doi:[10.1128/ecosalplus.esp-0028-2021](https://doi.org/10.1128/ecosalplus.esp-0028-2021) (2022).
21. Pinilla-Redondo, R. *et al.* Type IV CRISPR-Cas systems are highly diverse and involved in competition between plasmids. *Nucleic Acids Res.* **48**, 2000–2012. doi:[10.1093/nar/gkz1197](https://doi.org/10.1093/nar/gkz1197) (2020).
22. Rocha, E. P. C. & Bikard, D. Microbial defenses against mobile genetic elements and viruses: Who defends whom from what? *PLoS Biol.* **20**, e3001514. doi:[10.1371/journal.pbio.3001514](https://doi.org/10.1371/journal.pbio.3001514) (2022).
23. Pilosof, S. Conceptualizing microbeplasmid communities as complex adaptive systems. *Trends in Microbiology.* doi:[10.1016/j.tim.2023.01.007](https://doi.org/10.1016/j.tim.2023.01.007) (2023).
24. Zhu, S., Hong, J. & Wang, T. Horizontal gene transfer is predicted to overcome the diversity limit of competing microbial species. *Nat. Commun.* **15**, 800. doi:[10.1038/s41467-024-45154-w](https://doi.org/10.1038/s41467-024-45154-w) (2024).

25. Wang, T. & You, L. The persistence potential of transferable plasmids. *Nat. Commun.* **11**, 5589. doi:[10.1038/s41467-020-19368-7](https://doi.org/10.1038/s41467-020-19368-7) (2020).
26. Risely, A. *et al.* Host- plasmid network structure in wastewater is linked to antimicrobial resistance genes. *Nat. Commun.* **15**, 555. doi:[10.1038/s41467-024-44827-w](https://doi.org/10.1038/s41467-024-44827-w) (2024).
27. Bastolla, U. *et al.* The architecture of mutualistic networks minimizes competition and increases biodiversity. *Nature* **458**, 1018–1020. doi:[10.1038/nature07950](https://doi.org/10.1038/nature07950) (2009).
28. Thbault, E. & Fontaine, C. Stability of ecological communities and the architecture of mutualistic and trophic networks. *Science* **329**, 853–856. doi:[10.1126/science.1188321](https://doi.org/10.1126/science.1188321) (2010).
29. Pilosof, S., Porter, M. A., Pascual, M. & Kfi, S. The multilayer nature of ecological networks. *Nature Ecology and Evolution* **1**. doi:[10.1038/s41559-017-0101](https://doi.org/10.1038/s41559-017-0101) (2017).
30. Pilosof, S. *et al.* Competition for hosts modulates vast antigenic diversity to generate persistent strain structure in *Plasmodium falciparum*. *PLoS Biol.* **17**. doi:[10.1371/journal.pbio.3000336](https://doi.org/10.1371/journal.pbio.3000336) (2019).
31. Liaghat, A., Yang, J., Whitaker, R. & Pascual, M. Punctuated virus-driven succession generates dynamical alternations in CRISPR-mediated microbe-virus coevolution. *J. R. Soc. Interface* **21**, 20240195. doi:[10.1098/rsif.2024.0195](https://doi.org/10.1098/rsif.2024.0195) (2024).
32. Coyte, K. Z., Schluter, J. & Foster, K. R. The ecology of the microbiome: Networks, competition, and stability. *Science* **350**, 663–666. doi:[10.1126/science.aad2602](https://doi.org/10.1126/science.aad2602) (2015).
33. Li, L. *et al.* Dissecting the HGT network of carbon metabolic genes in soil-borne microbiota. *Front. Microbiol.* **14**, 1173748. doi:[10.3389/fmicb.2023.1173748](https://doi.org/10.3389/fmicb.2023.1173748) (2023).
34. Flores, C. O., Meyer, J. R., Valverde, S., Farr, L. & Weitz, J. S. Statistical structure of host-phage interactions. *Proc. Natl. Acad. Sci. U. S. A.* **108**, E288–97. doi:[10.1073/pnas.1101595108](https://doi.org/10.1073/pnas.1101595108) (2011).
35. Weitz, J. S. *et al.* Phage-bacteria infection networks. *Trends Microbiol.* **21**, 82–91. doi:[10.1016/j.tim.2012.11.003](https://doi.org/10.1016/j.tim.2012.11.003) (2013).
36. Beckett, S. J. & Williams, H. T. P. Coevolutionary diversification creates nested-modular structure in phage-bacteria interaction networks. *Interface Focus* **3**, 20130033. doi:[10.1098/rsfs.2013.0033](https://doi.org/10.1098/rsfs.2013.0033) (2013).
37. Fortuna, M. A. *et al.* Coevolutionary dynamics shape the structure of bacteria-phage infection networks. *Evolution* **73**, 1001–1011. doi:[10.1111/evo.13731](https://doi.org/10.1111/evo.13731) (2019).
38. Popa, O. & Dagan, T. Trends and barriers to lateral gene transfer in prokaryotes. *Curr. Opin. Microbiol.* **14**, 615–623. doi:[10.1016/j.mib.2011.07.027](https://doi.org/10.1016/j.mib.2011.07.027) (2011).
39. Popa, O., Landan, G. & Dagan, T. Phylogenomic networks reveal limited phylogenetic range of lateral gene transfer by transduction. *ISME J.* **11**, 543–554. doi:[10.1038/ismej.2016.116](https://doi.org/10.1038/ismej.2016.116) (2017).
40. Light, S., Kraulis, P. & Elovsson, A. Preferential attachment in the evolution of metabolic networks. *BMC Genomics* **6**, 159. doi:[10.1186/1471-2164-6-159](https://doi.org/10.1186/1471-2164-6-159) (2005).
41. Liu, Y. *et al.* Microbial community structure and ecological networks during simulation of diatom sinking. *Microorganisms* **10**, 639. doi:[10.3390/microorganisms10030639](https://doi.org/10.3390/microorganisms10030639) (2022).
42. Rawstern, A. H., Hernandez, D. J. & Afkhami, M. E. Hub taxa are keystone microbes during early succession. *bioRxiv*, 2023.03.02.530218. doi:[10.1101/2023.03.02.530218](https://doi.org/10.1101/2023.03.02.530218) (2023).

43. Yang, C. H. & Jung, H. Topological dynamics of the 2015 South Korea MERS-CoV spread-on-contact networks. *Sci. Rep.* **10**. doi:[10.1038/s41598-020-61133-9](https://doi.org/10.1038/s41598-020-61133-9) (2020).
44. Haegeman, B. & Etienne, R. S. Relaxing the zero-sum assumption in neutral biodiversity theory. *J. Theor. Biol.* **252**, 288–294. doi:[10.1016/j.jtbi.2008.01.023](https://doi.org/10.1016/j.jtbi.2008.01.023) (2008).
45. Lopatkin, A. J. *et al.* Persistence and reversal of plasmid-mediated antibiotic resistance. *Nat. Commun.* **8**, 1689. doi:[10.1038/s41467-017-01532-1](https://doi.org/10.1038/s41467-017-01532-1) (2017).
46. Amor, D. R., Ratzke, C. & Gore, J. Transient invaders can induce shifts between alternative stable states of microbial communities. *Sci. Adv.* **6**, eaay8676. doi:[10.1126/sciadv.aay8676](https://doi.org/10.1126/sciadv.aay8676) (2020).
47. Schaal, K. A. *et al.* Species interactions determine plasmid persistence in a 3-member bacterial community. *bioRxiv*. doi:[10.1101/2025.05.31.657151](https://doi.org/10.1101/2025.05.31.657151) (2025).
48. Lam, M. M. C. *et al.* Convergence of virulence and MDR in a single plasmid vector in MDR *Klebsiella pneumoniae* ST15. *J. Antimicrob. Chemother.* **74**, 1218–1222. doi:[10.1093/jac/dkz028](https://doi.org/10.1093/jac/dkz028) (2019).
49. Wang, X. *et al.* Inter-plasmid transfer of antibiotic resistance genes accelerates antibiotic resistance in bacterial pathogens. *ISME J.* **18**. doi:[10.1093/ismejo/wrad032](https://doi.org/10.1093/ismejo/wrad032) (2024).
50. Kauffman, K. M. *et al.* Resolving the structure of phage-bacteria interactions in the context of natural diversity. *Nat. Commun.* **13**, 372. doi:[10.1038/s41467-021-27583-z](https://doi.org/10.1038/s41467-021-27583-z) (2022).
51. Biggs, C. R. *et al.* Does functional redundancy affect ecological stability and resilience? A review and metaanalysis. *Ecosphere* **11**. doi:[10.1002/ecs2.3184](https://doi.org/10.1002/ecs2.3184) (2020).
52. Wood, Z. T., Palkovacs, E. P., Olsen, B. J. & Kinnison, M. T. The importance of Eco-evolutionary potential in the anthropocene. *Bioscience* **71**, 805–819. doi:[10.1093/biosci/biab010](https://doi.org/10.1093/biosci/biab010) (2021).
53. Puente-Sánchez, F., Pascual-García, A., Bastolla, U., Pedrós-Ali, C. & Tamames, J. Cross-biome microbial networks reveal functional redundancy and suggest genome reduction through functional complementarity. *Commun. Biol.* **7**, 1046. doi:[10.1038/s42003-024-06616-5](https://doi.org/10.1038/s42003-024-06616-5) (2024).
54. Santos-Lopez, A. *et al.* A naturally occurring single nucleotide polymorphism in a multicopy Plasmid produces a reversible increase in antibiotic resistance. *Antimicrob. Agents Chemother.* **61**, AAC.01735–16. doi:[10.1128/AAC.01735-16](https://doi.org/10.1128/AAC.01735-16) (2017).
55. Harrison, E. *et al.* Bacteriophages limit the existence conditions for conjugative plasmids. *MBio* **6**. doi:[10.1128/mBio.00586-15](https://doi.org/10.1128/mBio.00586-15) (2015).
56. Neil, K., Allard, N. & Rodrigue, S. Molecular mechanisms influencing bacterial conjugation in the intestinal Microbiota. *Front. Microbiol.* **12**, 673260. doi:[10.3389/fmicb.2021.673260](https://doi.org/10.3389/fmicb.2021.673260) (2021).

## Supplementary Figures

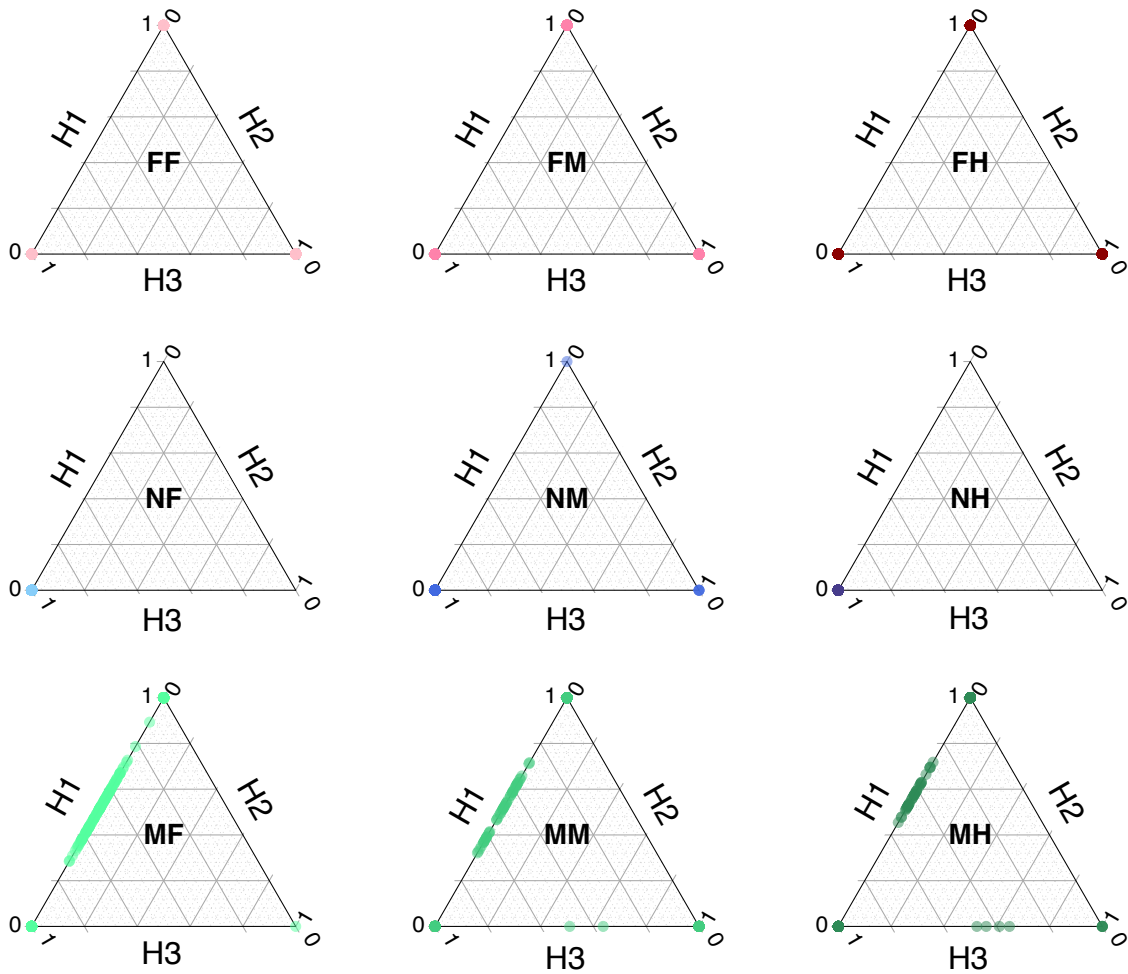


**Figure S1:** Relative abundance of populations at the end of the simulations ( $t = 20000$  hours) at the following network structures: full I x full P (FF), full I x modular P (FM), full I x hub P (FH), nested I x full P (NF), nested I x modular P (NM), nested I x hub P (NH), modular I x full P (MF), modular I x modular P (MM), and modular I x hub P (MH). Dots on the vertices represent no coexistence (i.e. only one population survived), while dots on the edges represent the coexistence of two populations.

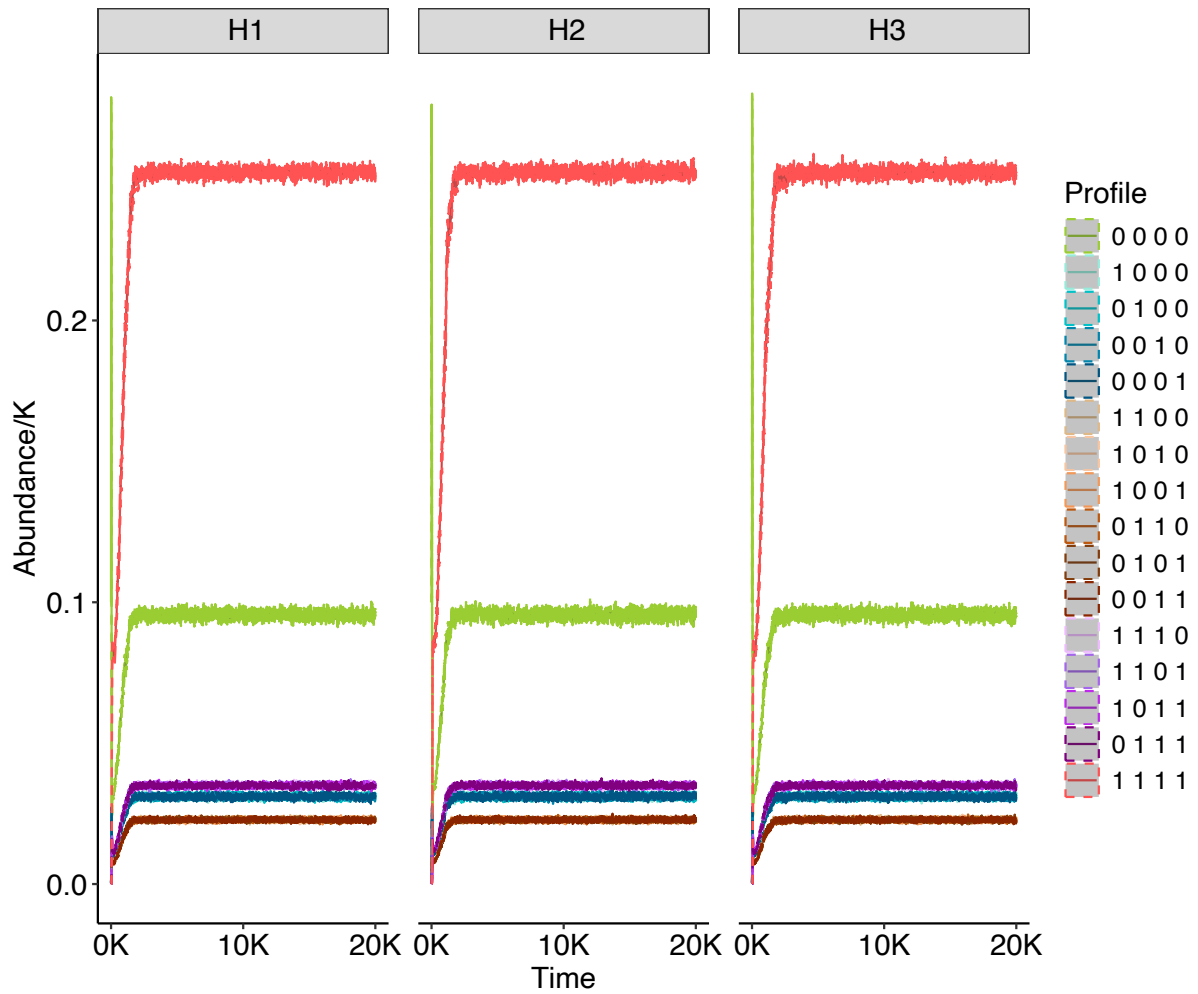


**Figure S2:** Dynamics of subpopulation abundance (mean  $\pm$  1 SE) at full I x full P (FF). Note that the number of replicates of a subpopulation at a given time point may vary across time, for it depends on how many replicates still have that subpopulation at that time point. The K at y-axis represents carrying capacity, while the K at x-axis represents 1000 (hours).

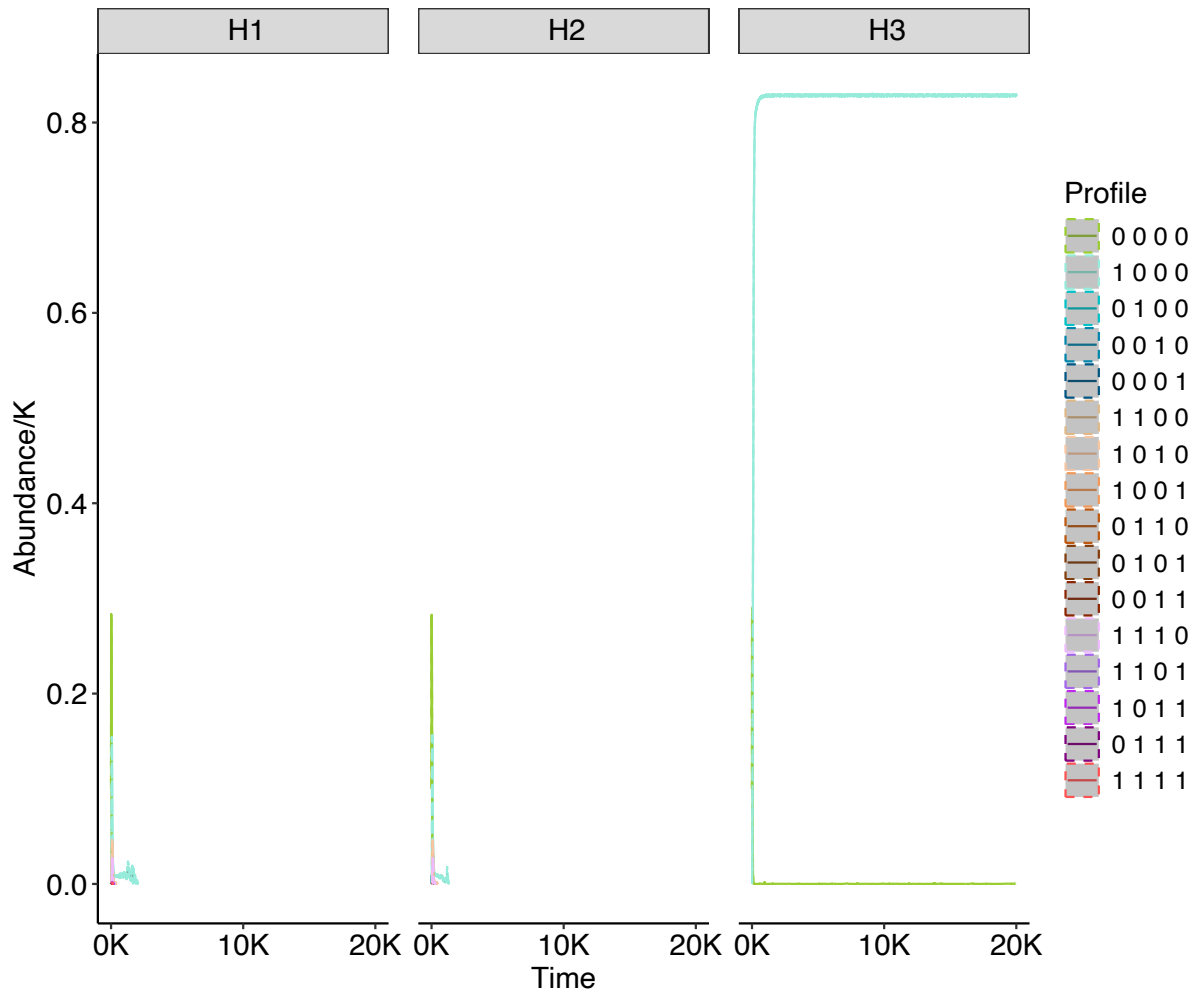


**Figure S3:** Dynamics of subpopulation abundance (mean  $\pm$  1 SE) at nested I x full P (NF). Note that the number of replicates of a subpopulation at a given time point may vary across time, for it depends on how many replicates still have that subpopulation at that time point. The K at y-axis represents carrying capacity, while the K at x-axis represents 1000 (hours).

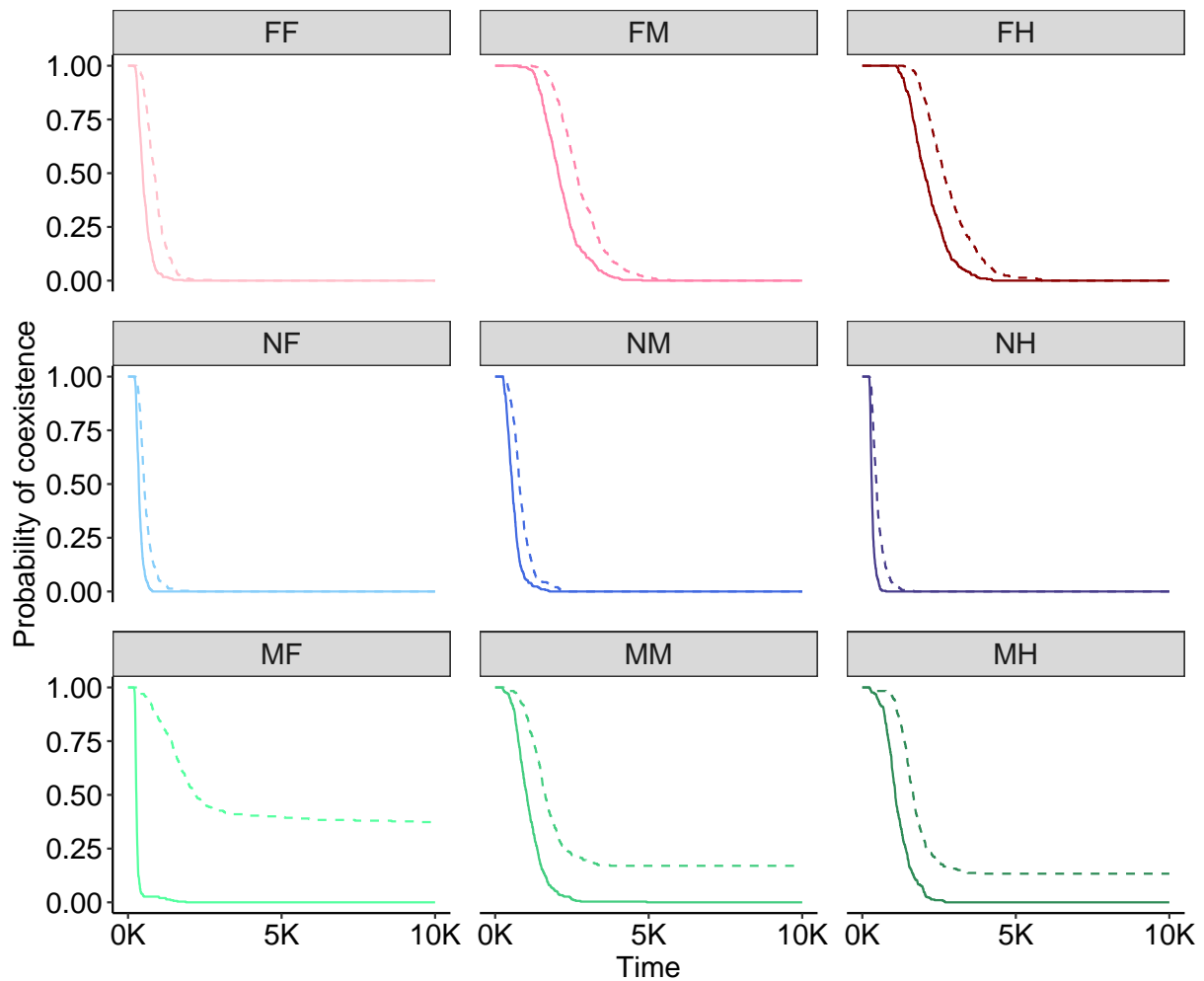


**Figure S4:** Dynamics of microbe coexistence of three populations (solid line) and two populations (dashed line) at the end of the simulations ( $t = 20000$  hours) at the following network structures: full I x full P (FF), full I x modular P (FM), full I x hub P (FH), nested I x full P (NF), nested I x modular P (NM), nested I x hub P (NH), modular I x full P (MF), modular I x modular P (MM), and modular I x hub P (MH). The dynamics of microbe coexistence probability is calculated as the proportion of replicates with complete(3-population)/partial(2-population) coexistence out of total number of replicates across time. Time was only plotted to  $t = 10000$  where all probabilities had dropped to zero. The K at x-axis represents 1000 (hours).

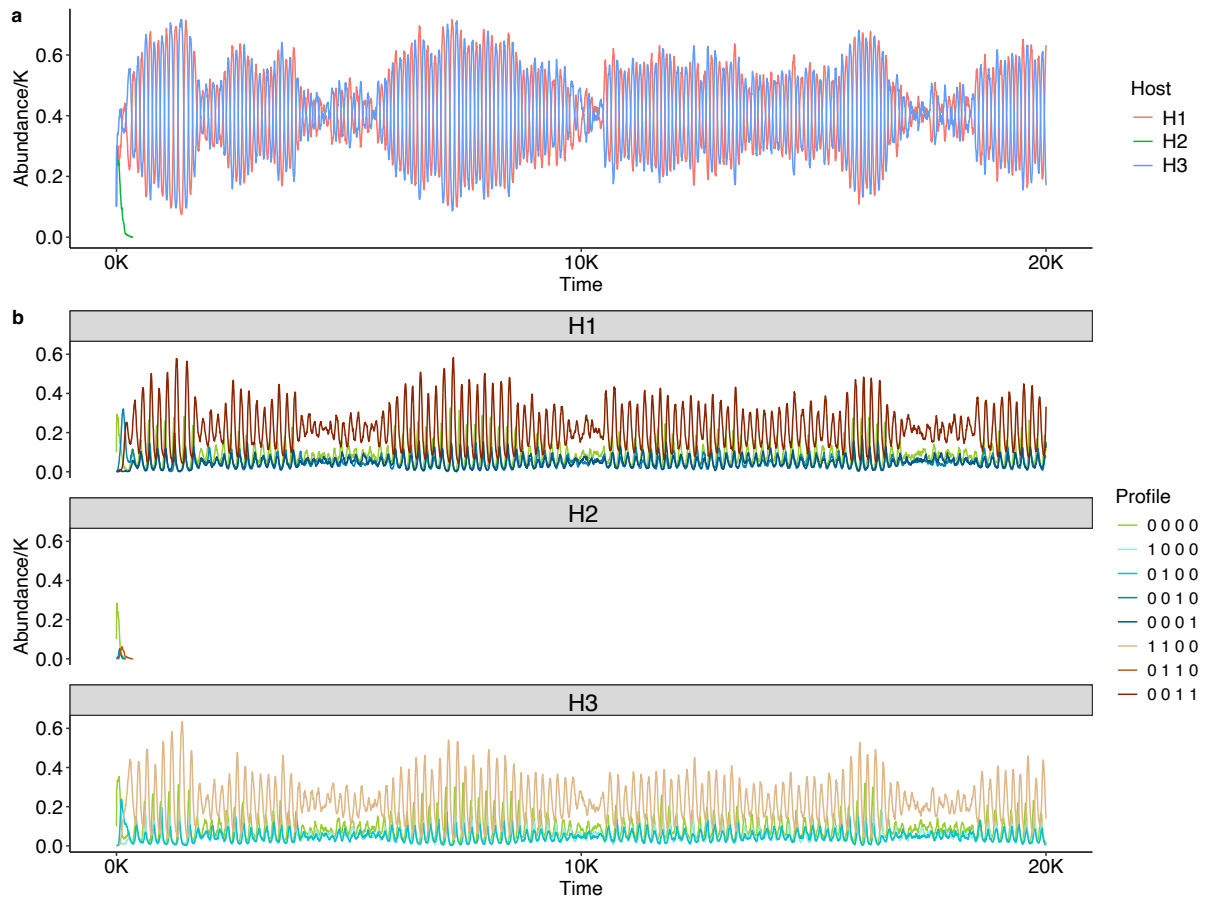


**Figure S5:** Dynamics of population abundance (a) and subpopulation abundance (b) at modular I x full P (MF) from replicate 21. Replicate 21 demonstrated the stable coexistence scenario where the plasmid-free subpopulations of the peripheral hosts persisted. The K at y-axis represents carrying capacity, while the K at x-axis represents 1000 (hours).

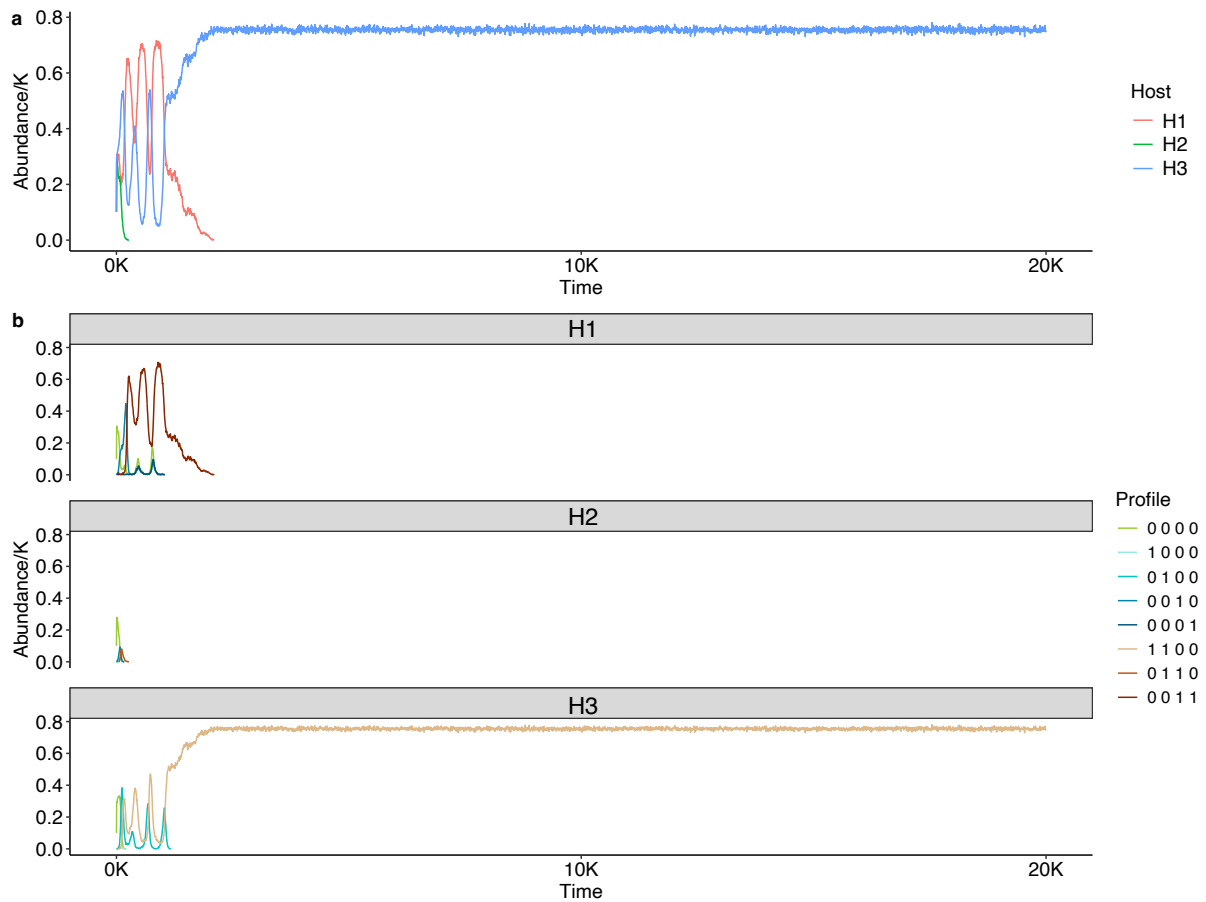


**Figure S6:** Dynamics of population abundance (a) and subpopulation abundance (b) at modular I x full P (MF) from replicate 23. Replicate 23 demonstrated the unstable coexistence scenario where the plasmid-free subpopulations of the peripheral hosts went extinct. When the plasmid-free subpopulations went extinct, monoplasmidic subpopulations lost input from infection and quickly got co-infected, destabilizing the oscillatory dynamics of the coexisting populations. The K at y-axis represents carrying capacity, while the K at x-axis represents 1000 (hours).

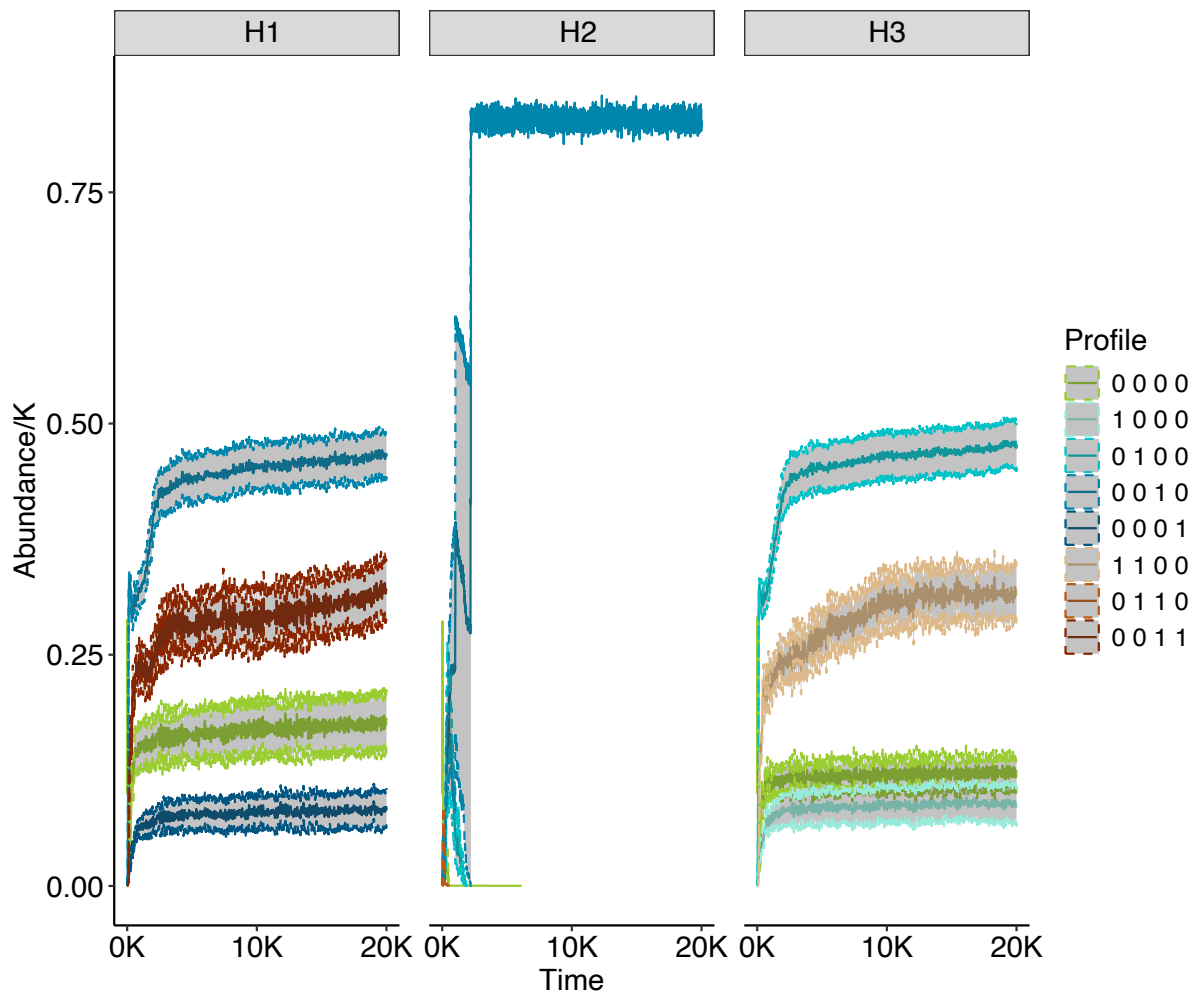


**Figure S7:** Dynamics of subpopulation abundance (mean  $\pm$  1 SE) at modular I x full P (MF). Note that the number of replicates of a subpopulation at a given time point may vary across time, for it depends on how many replicates still have that subpopulation at that time point. The K at y-axis represents carrying capacity, while the K at x-axis represents 1000 (hours).

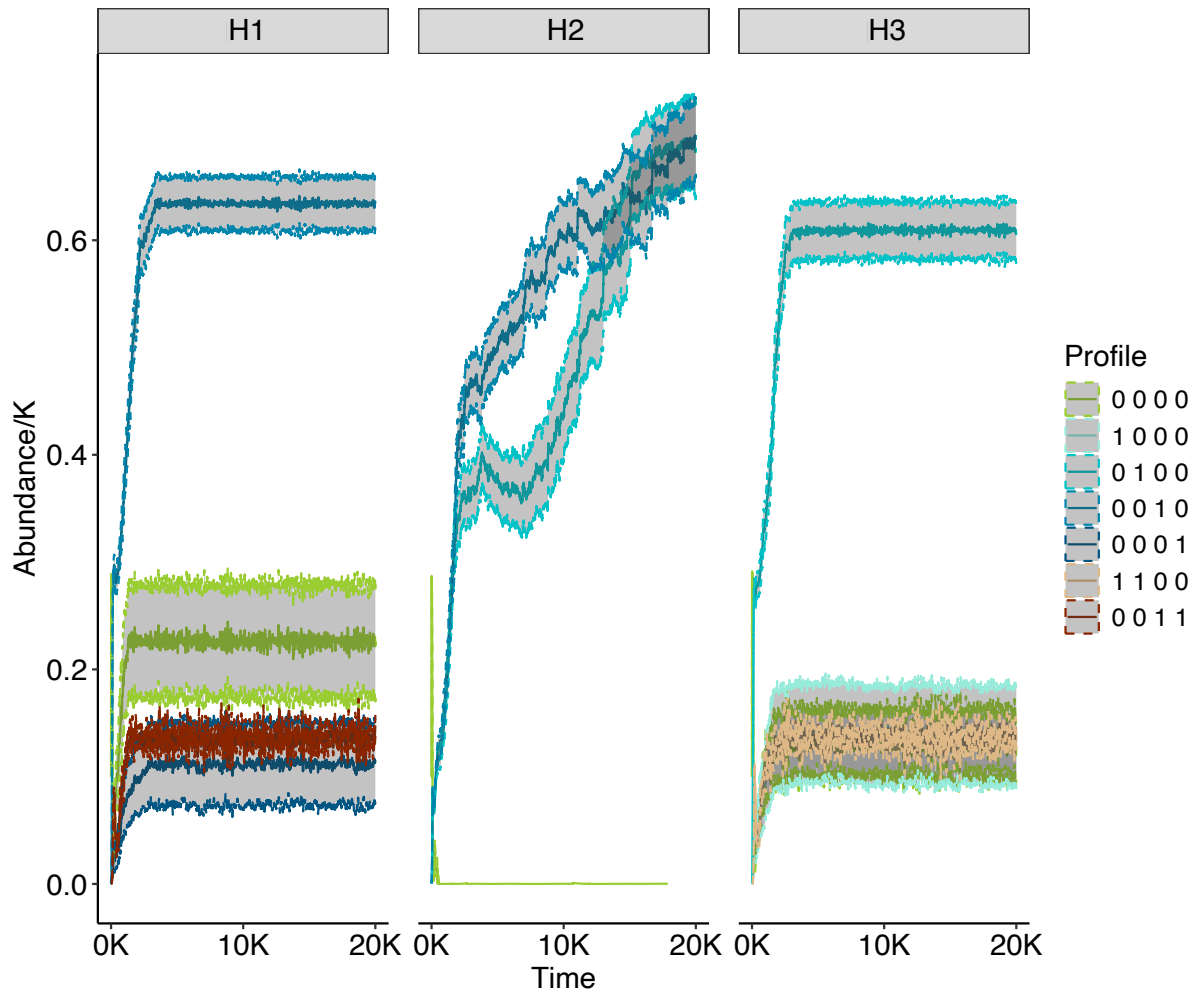


**Figure S8:** Dynamics of subpopulation abundance (mean  $\pm$  1 SE) at modular I x modular P (MM). Note that the number of replicates of a subpopulation at a given time point may vary across time, for it depends on how many replicates still have that subpopulation at that time point. The K at y-axis represents carrying capacity, while the K at x-axis represents 1000 (hours).

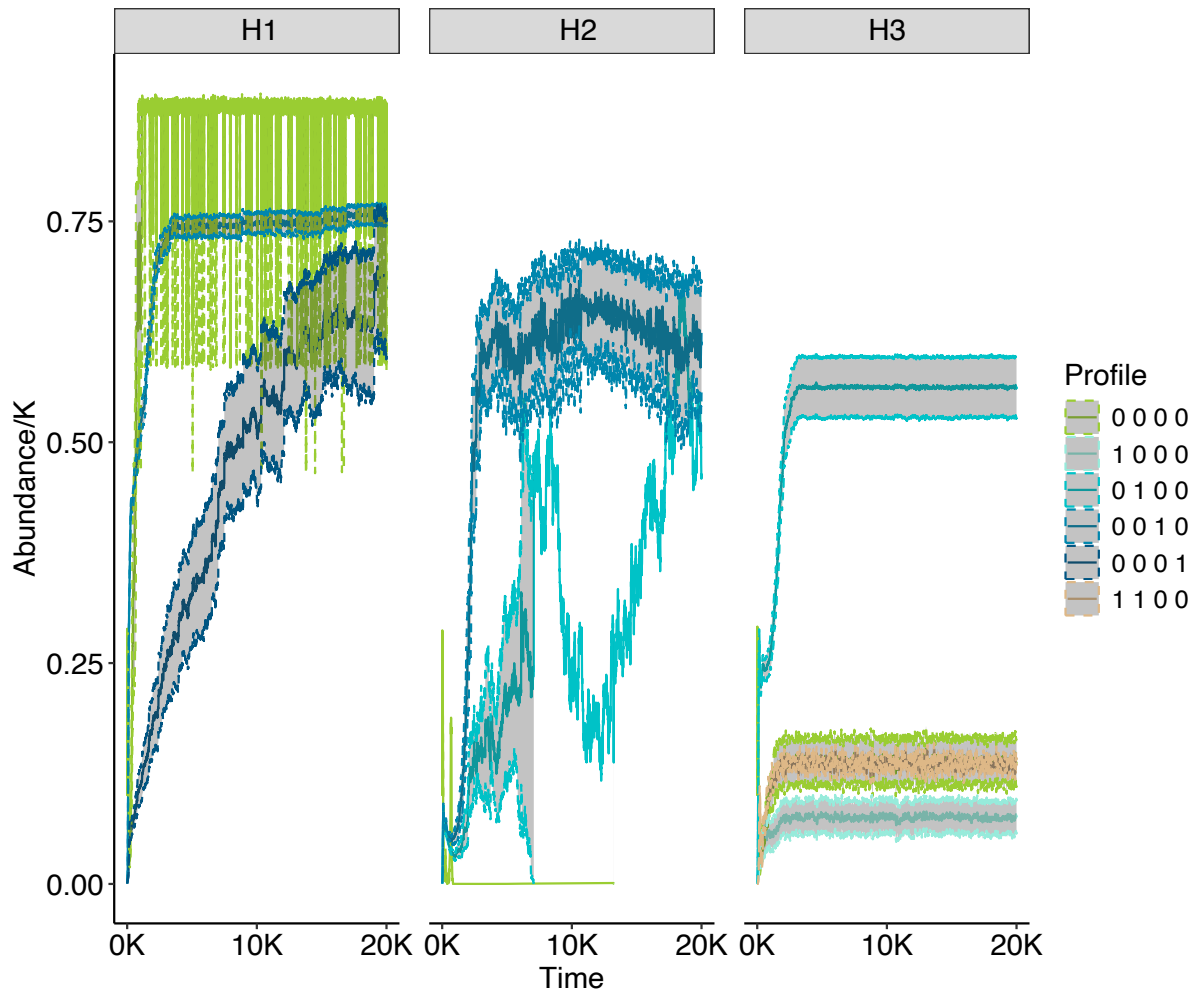


**Figure S9:** Dynamics of subpopulation abundance (mean  $\pm$  1 SE) at modular I x hub P (MH). Note that the number of replicates of a subpopulation at a given time point may vary across time, for it depends on how many replicates still have that subpopulation at that time point. The K at y-axis represents carrying capacity, while the K at x-axis represents 1000 (hours).

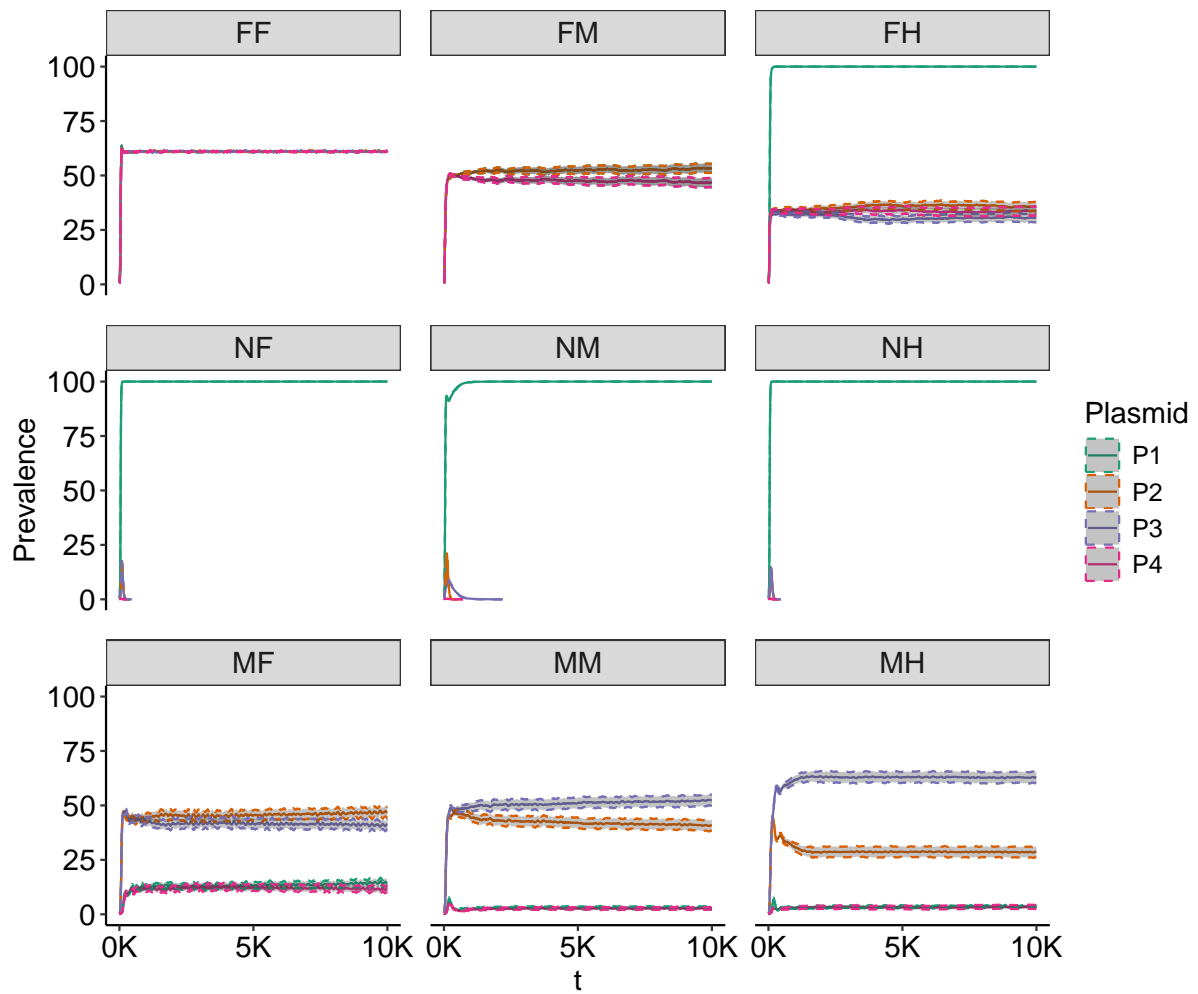


**Figure S10:** Dynamics of plasmid prevalence (mean  $\pm$  1 SE) at the following network structures: full I x full P (FF), full I x modular P (FM), full I x hub P (FH), nested I x full P (NF), nested I x modular P (NM), nested I x hub P (NH), modular I x full P (MF), modular I x modular P (MM), and modular I x hub P (MH). Time was only plotted to  $t = 10000$  where equilibrium of plasmid prevalence had been reached. The K at x-axis represents 1000 (hours).

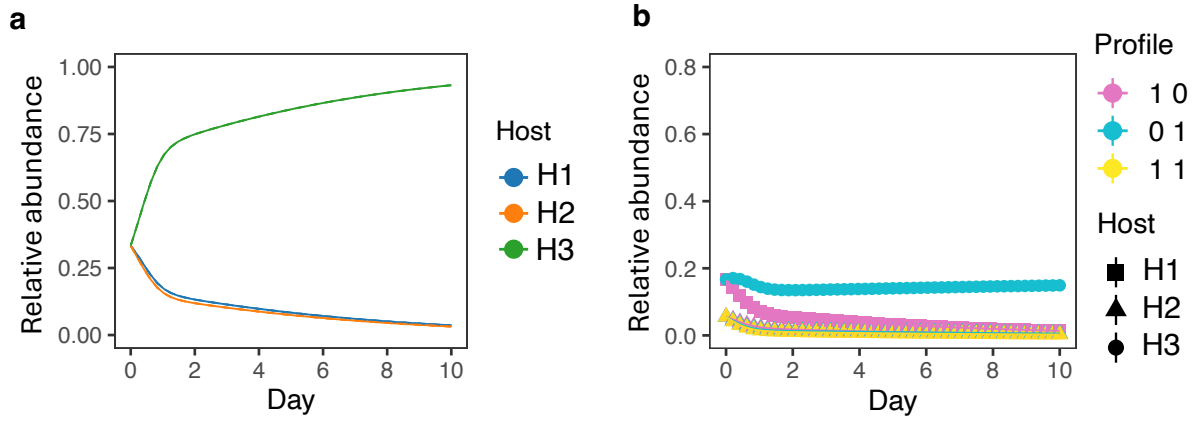


**Figure S11:** (a) The host population dynamics and (b) host subpopulation dynamics from the simulations assuming no increase on the growth rate of the bridge host H2 under a modular **I** based on an empirical system (Figure 5a, top row).

## Supplementary Methods and Tables

Below are the supplementary materials for the mathematical formalism of the ABM and parameter settings for simulations based on empirical data. For original Julia and R scripts, input JSON files, and output SQLite files, please visit: [https://github.com/HFSP-EcoNets/ABM\\_code](https://github.com/HFSP-EcoNets/ABM_code).

### S1 Parameters for the simulations based on empirical data

**Table S1:** Host-specific parameters. The net population growth rates were parameterized using the empirical data fit to the standard form of logistic equation in the R package *growthcurver* (Sprouffske 2020), while the population growth rates and death rates were arbitrarily assigned to match the net population growth rate. The infection rates and competition coefficients were assigned in a relative magnitude in order to better match the empirical subpopulation and population dynamics. The segregation rates and perturbation impact were arbitrarily assigned and fixed to an extremely low value as these can be omitted. The community-wise carrying capacity was arbitrarily assigned for computational efficiency. We later assumed an increase in the growth rate of the bridge host (H2).

Host traits	H1	H2	H3
growth rate $\eta_i$	0.1	0.15*	0.2
death rate $\mu_i$	0.01	0.01	0.01
infection rate $\phi_{i,p}$	5e-9	5e-9	5e-8
segregation rate $e_i$	1e-8	1e-8	1e-8
competition coefficient on H1 $a_{1i}$	1	0.02	0.03
competition coefficient on H2 $a_{2i}$	5e-3	1	0.03
competition coefficient on H3 $a_{3i}$	5e-3	0.02	1
perturbation impact $\epsilon_i$	0	0.0	0.0
community-wise carrying capacity $K$	1e5	1e5	1e5

\* Set to 0.1 under the assumption of no increase in the growth rate of H2.

**Table S2:** Plasmid-specific parameters. The plasmid costs were assigned in a relative magnitude based on empirical monocultures of the infected bridge host population in order to better match the empirical subpopulation and population dynamics. The plasmid resistance was arbitrarily assigned and fixed as these are irrelevant for systems without perturbations.

Plasmid traits	P1	P2
plasmid cost $c_\alpha$	0.2	0.4
plasmid resistance $\rho_\alpha$	0.7	0.7

**Table S3:** Initial abundance of the plasmid-present system for a modular infection network **I**

Host $i$	Plasmid profile $p$	Abundance $H_{i,p}$
1	[0,0]	1650
1	[1,0]	1650
2	[0,0]	1650
2	[1,0]	550
2	[0,1]	550
2	[1,1]	550
3	[0,0]	1650
3	[0,1]	1650

**Table S4:** Initial abundance of the plasmid-present system for a full infection network **I**

Host $i$	Plasmid profile $p$	Abundance $H_{i,p}$
1	[0,0]	1650
1	[1,0]	550
1	[0,1]	550
1	[1,1]	550
2	[0,0]	1650
2	[1,0]	550
2	[0,1]	550
2	[1,1]	550
3	[0,0]	1650
3	[1,0]	550
3	[0,1]	550
3	[1,1]	550

## S2 Variable glossary

The variables (including constants and parameters) for the ABM are introduced in Table S5.

**Table S5:** Constants and parameters for the ABM

Variable	Definition	Type
$t$	time	float
$t_{final}$	time scale of the simulation	float (h)
$n_b$	number of host populations in the system	integer
$n_p$	number of plasmids in the system	integer
$i, j, k$	host of the entity	integer
$p, q, r$	plasmid profile of the entity	integer
$\alpha$	plasmid $\alpha$	integer
$H_{i,p}$	entity and abundance of a host subpopulation	integer
$H_i$	abundance of host $i$	integer
$K$	community-wise carrying capacity of host	float
$e_i$	probability of segregation error of host $i$	float
$\mu_i$	per capita death rate of host $i$	float
$\eta_i$	per capita growth rate of host $i$	float
$\phi_{i,p}$	per capita infection rate of host subpopulation $H_{i,p}$	float
$\gamma_{i,p}$	infection coefficient of host subpopulation $H_{i,p}$	float
$\rho_\alpha$	resistance of plasmid $\alpha$	float
$c_\alpha$	cost of plasmid $\alpha$ on host growth	float
<b>A</b>	host competition matrix	matrix of floats
<b>H</b>	HGT matrix	matrix of floats
<b>I</b>	infection matrix	matrix of integers
<b>P</b>	plasmid compatibility matrix	matrix of integers
<b><math>\Gamma</math></b>	propensity tensor of infection	3-D tensor of floats

## S3 Subpopulation dynamics

The simplified dynamics of plasmid-infected and plasmid-free subpopulations are illustrated in Figure S12. Each subpopulation experiences events that lead to an increase or decrease in abundance at subpopulation-specific per capita rates. Note that for plasmid infection, the infection rate only determines the frequency of infection events, while the rate-independent propensity tensor  $\Gamma$  determines the propensity at which an individual of a given type of plasmid-carrying subpopulation is produced. The equations and related parameters of the per capita rates and the propensity tensor are described in Methods.

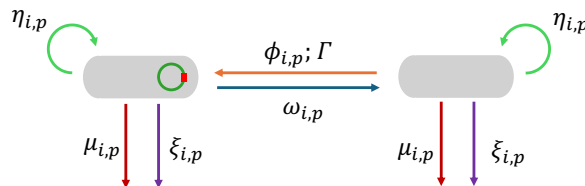


**Figure S12:** Illustration of the dynamics of plasmid-carrying subpopulation (left box with a circle in it) and plasmid-free subpopulation (right box). Colored arrows indicate abundance inflows/outflows from the five events: growth (green), death (red), competition (purple), infection (orange), and segregation (blue). Alongside each arrow lists the per capita rate of the event, with subscripts denoting host  $i$  and plasmid profile  $p$  of the subpopulation.

## S4 Input and output

The raw simulation input is in JSON format and includes the variables described in Table S6.

The raw simulation output is in SQLite format and includes three tables. Table "bsub-abundance" is the table of host subpopulation dynamics. It includes time (**t**), subpopulation id (**subpop\_id**), host id, plasmid profile (**p\_profile**), and sub-population abundances (**abundance**). Table "events" includes time (**t**), the accumulated number of growth events (**growth**), death events (**death**), segregation events (**segregation**), competition events (**competition**), and infection events (**infection**). Table "meta" includes the general information about the simulation: **seed**, **key** (the id of a simulation and output assigned by the experiment designer), **job** (the id of the job generated by the HPC), **start time**, **end time**, and **elapsed seconds**.

**Table S6:** Variables for the ABM input

Condition	Content	Type (v(): vector of ())
<b>t_final</b>	t at which simulation ends	float
<b>t_output</b>	the t interval after which state is recorded	float
<b>rng_seed</b>	seed for the simulation	null;float
<b>n_seeds</b>	the number of seed for the simulation	integer; 1
<b>n_bstrains</b>	$n_b$ maximum number of host populations in the system	integer
<b>n_pstrains</b>	$n_p$ maximum number of plasmids in the system	integer
<b>n_bsubstrains</b>	number of subpopulations at initial state	integer
<b>strain_id_for_each_substrain</b>	host id $i$ of subpopulations	integer
<b>n_ind_bsubstrains</b>	abundance of subpopulations	integer
<b>p_profile_bsubstrains</b>	the plasmid profile $p$ of subpopulations	v(v(s) of binary element(s))
<b>growth_rate</b>	host-specific growth rate $\eta_i$	v(float)
<b>death_rate</b>	host-specific death rate $\mu_i$	v(float)
<b>carrying_capacity</b>	$K$	v(integer)
<b>infection_rate</b>	host-specific infection coefficient $\gamma_i$	v(float)
<b>segregation_error</b>	host-specific rate of segregation error $e_i$	v(float(s))
<b>perturbation_impact</b>	host-specific degradation coefficient $k_i$	v(float/0 w/o perturbation)
<b>plasmid_resistance</b>	plasmid-specific plasmid resistance $\rho_\alpha$	v(float)
<b>plasmid_cost</b>	plasmid-specific plasmid cost $c_\alpha$	v(float)
<b>A</b>	host competition matrix <b>A</b>	v(v(float))
<b>H</b>	host HGT matrix <b>H</b>	v(v(integer))
<b>I</b>	plasmid infection matrix <b>I</b>	v(v(float(s)))
<b>P</b>	plasmid compatibility matrix <b>P</b>	v(v(float))
<b>tensor_file</b>	path to the JSON file of the propensity tensor	character

## S5 Complexity-dependent computational efficiency

To demonstrate how the system complexity limits the computational efficiency of our model, we ran a model performance test across n-host-n-plasmid systems where n ranged from one to six. Each n-host-n-plasmid system was initialized with  $n \times (n + 1)$  subpopulations, where each host population had a plasmid-free subpopulation with 1000 individuals, and all potential single-plasmid-carrying subpopulations with 100 individuals each. We fixed all the host and plasmid traits across populations, applied the reference (full) structure for all interaction networks, and increased the community-wide carrying capacity  $K$  linearly with the initial number of subpopulations (Table S7). The elapsed time for the infection tensor  $\mathbf{\Gamma}$  generation, initialization and simulation substantially increased with system complexity (Fig. S13).

**Table S7:** Constants and parameters for the model performance test

Variable	Definition	Value
$t_{final}$	time scale of the simulation	500
$n$	number of host and plasmid populations in the system	1:6
$K$	community-wise carrying capacity of host	1e4:2.1e5
$e_i$	probability of segregation error of host $i$	e-8
$\mu_i$	per capita death rate of host $i$	0.015
$\eta_i$	per capita growth rate of host $i$	1.0
$\gamma_{i,p}$	infection coefficient of host subpopulation $H_{i,p}$	1e-4
$\rho_\alpha$	resistance of plasmid $\alpha$	1.0
$c_\alpha$	cost of plasmid $\alpha$ on host growth	0.02
<b>A</b>	host competition matrix	$n \times n$ matrix of 1s
<b>H</b>	HGT matrix	$n \times n$ matrix of 1s
<b>I</b>	infection matrix	$n \times n$ matrix of 1s
<b>P</b>	plasmid compatibility matrix	$n \times n$ matrix of 1s and off-diagonal 0s

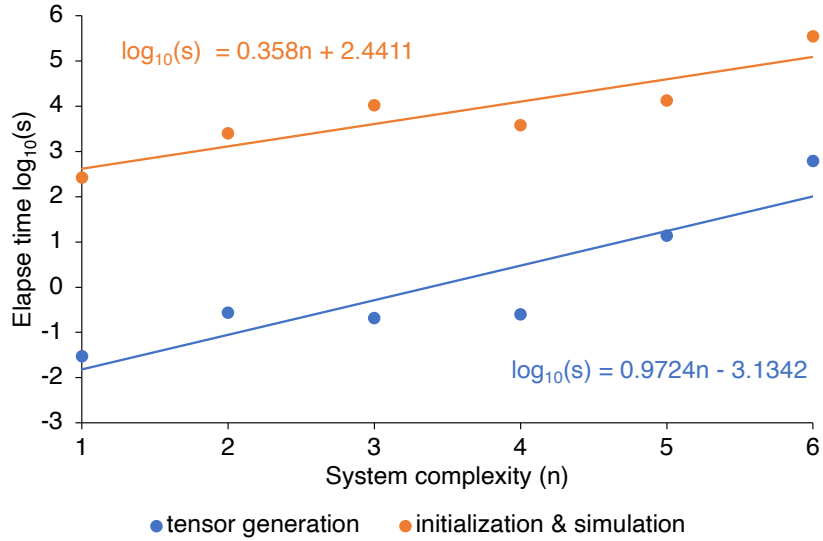


**Figure S13:** Elapse time of tensor generation, initialization and simulation across system complexity  $n$ , i.e. the number of host and plasmid populations in the system.

## References

Sprouffske K (2020). growthcurver: Simple Metrics to Summarize Growth Curves. R package version 0.3.1, <https://CRAN.R-project.org/package=growthcurver>.